NTNU

Norwegian University of
Science and Technology

Time domain simulations of wind turbine blade installation using a floating installation vessel

Aurelien Lorenzo Edy

Marine Technology
Submission date: July 2017
Supervisor: Zhen Gao, IMT

Norwegian University of Science and Technology
Department of Marine Technology

Time Domain Simulations of Wind Turbine Blade Installation using a Floating Installation Vessel

Aurélien Edy

July 2017

MASTER THESIS

Department of Marine Technology

Norwegian University of Science and Technology

Supervisor: Professor Zhen Gao

Co-supervisors: Doctor Zhengshun Chen

Phd Yuna Zhao

Preface

This report is not only the concluding work of my Master of Science in Marine Technology at the Department of Marine Technology of NTNU, it is also the conclusion of my double degree diploma made in partnership with the French École Centrale Nantes. At Centrale Nantes, I studied during two years a wide range of engineering fields, including a specialization in hydrodynamics, and some soft skills sciences, from management to finance. In the following two years, I learned about Marine Technology at NTNU, with a specialization in marine structures.

During the spring semester 2017, this thesis was carried out under the supervision of Zhen Gao with the weekly help of Yuna Zhao and Zhengshun Cheng. It is aimed to assess the feasibility of an innovative method for installation of offshore wind turbine's blades. This work is part of a bigger analysis of the use of floating vessels for installation of offshore wind farms.

To read this report, basic knowledges on sea loads, aerodynamics, sea state statistics and marine operations are required. The specific theory models implemented in this paper are described, and definition of technical vocabulary is included.

Trondheim, 2017-07-03

Aurélien Edy

Acknowledgment

A Master thesis is a long and personal task that cannot be achieved without help. It closes the final chapter of my engineering studies, and I am using this section to thank the persons that I owe the successful completion of this thesis.

Firstly, I would like to express my sincere gratefulness to Professor Zhen Gao, my supervisor in NTNU's Department of Marine Technology, for giving me the precious opportunity to work on this fascinating topic, guiding me with his vast knowledge and providing relevant answers to all my questions.

I also want to thank Yuna Zhao and Zhengshun Cheng for their weekly help and supervision of the path I was taking with my thesis. Their valuable advice coupled to the guidance of Pr. Gao were fundamental to the realization of this thesis. Yuna's help was very precious for learning to use the SIMA software and handling the theoretical and numerical models requested for my work. I would like to recognize also Zhengshun's inputs for the simulation of the aerodynamic behavior of lifted objects.

Finally, I would like to thank my family and my friends for being always supportive.

A.E.

Summary and Conclusions

This paper is aimed to assess the feasibility of the mating of the blade of an OWT by a floating installation vessel. A state of the art analysis of the current practices in the industry shows that jack-up vessels are preferred when it comes to top turbine installation. As the mating of the top turbine components happens at large heights and needs a high degree of precision, the use of jack-up crane vessels that have no wave-induced motions seems relevant. However, the drawbacks of the jack-up operations, such as the important time spent in the leg deployment and the costs of such operations, motivated the writer of this thesis to look for other innovative installation methods. The modeling of a innovative design of tower ring concept, introduced by De Groot (2015), is realized to assess the feasibility of blade mating with floating vessel. This modeling, performed with the use of the software SIMO, leads to the establishment of the limiting environmental conditions for performing the operation. The results show that the impact of the turbulent wind on the lifted blade is not as critical as the impact of the vessel motions due to the waves. These wave-induced motions are even more critical when the waves are coming from the side of the moored installation vessel.

The comparison with the jack-up installation shows that jack-up operations accept limiting sea states of wider significant wave heights and peak periods than the floating vessel installation. One additional problem of the floating vessel is the effect of the mean wave direction, which can limit drastically the allowable sea states when the vessel is not facing the waves. However, the operational time with floating vessels is almost divided by half for a total wind turbine installation compared with the jack-up vessels. The relevance of floating vessels for OWT installation must therefor continue to be investigated.

Contents

Chapter 1

Introduction

1.1 Background

As the world is leading towards more renewable energy in the global energy share, wind energy is perceived to be a major way of implementing the green transition. Consequently, the demand for energy extracted from wind is expected to increase in the future, but traditional onshore energy is not going to be sufficient. Indeed, the limitations for transporting the wind components on the traffic network on the size of blades and other turbine's components prevent designers to produce more powerful turbines. Another limitation of onshore wind farms is their impact on environment, and especially on the neighboring habitations due to noise and visibility pollution. It is thus hard to find appropriate areas for installing big wind farms.

At the opposite end of the scale, there is much more available space in the oceans and seas, and offshore wind is also stronger and more predictable than onshore. Wind conditions at sea are very adapted to wind turbines, with high wind speeds and low turbulences, mainly due to the fact that oceans are an open space that interferes only slightly with wind development.

Offshore wind-farms have been installed since the beginning of the 90's, and the past years have seen the development of offshore wind industry in Europe (Figure 1.1) and around the world. The EU community has proposed that the energy from renewables shall be at least 20% in 2020 and 50% in 2050 (Madland, 2012). However, with installed capacity now capable of producing approximately 40.6 TWh in a normal wind year, there is electricity from offshore wind to cover only 1.5% of the EU's total electricity consumption (EWEA, 2016). The expectations are

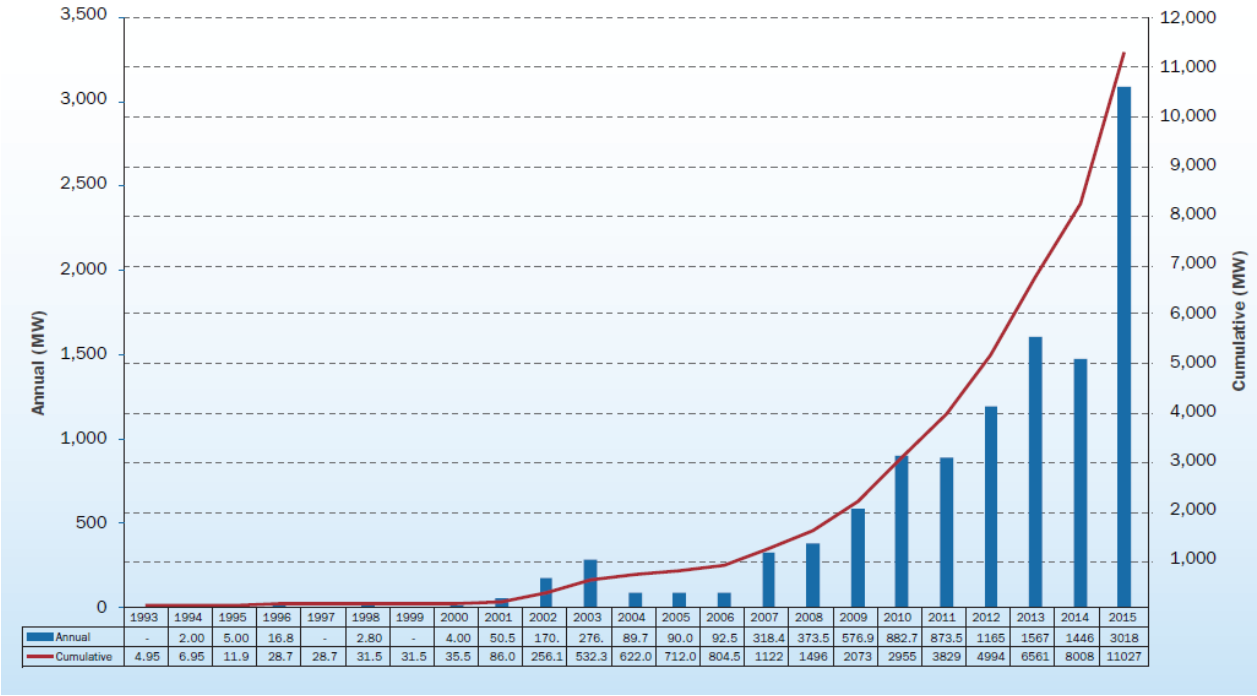

Figure 1.1: Cumulative and annual offshore wind installations in Europe (EWEA, 2016)

thus that the industry will continue to grow in the coming years.

For the moment, there are two different categories of offshore wind turbines being developed, floating and bottom-fixed. Floating wind turbines, whose costs are largely dependent on water depth, are more relevant for high depth. Bottom fixed wind turbines however, are attached to the seabed, and the environmental forces (i.e. forces from wind, waves and current) acting on the structure are effectively taken up by the soil beneath the seabed. They are efficient for small water depth, but costs for foundations and installations become too high above 50 to 100 meters.

As the wind offshore energy is getting bigger, new farm projects aim for bigger turbines, and longer distances to shore (Figure 1.2), in order to maximize profits and reduce the share of fixed costs in the total capex. This trend is the result of the importance of foundation and installation costs in the overall costs, in contrary to onshore wind industry. Indeed, for an OWT, installation is up to 20% of capital cost. There is a huge challenge in reducing installation cost and installation time, and new methods must therefore be evaluated. For a bottom-fixed turbine, installation is usually divided in two parts. First occurs the installation of the foundation, and afterward the installation of the tower, nacelle and blades. Usually, installation vessels for the

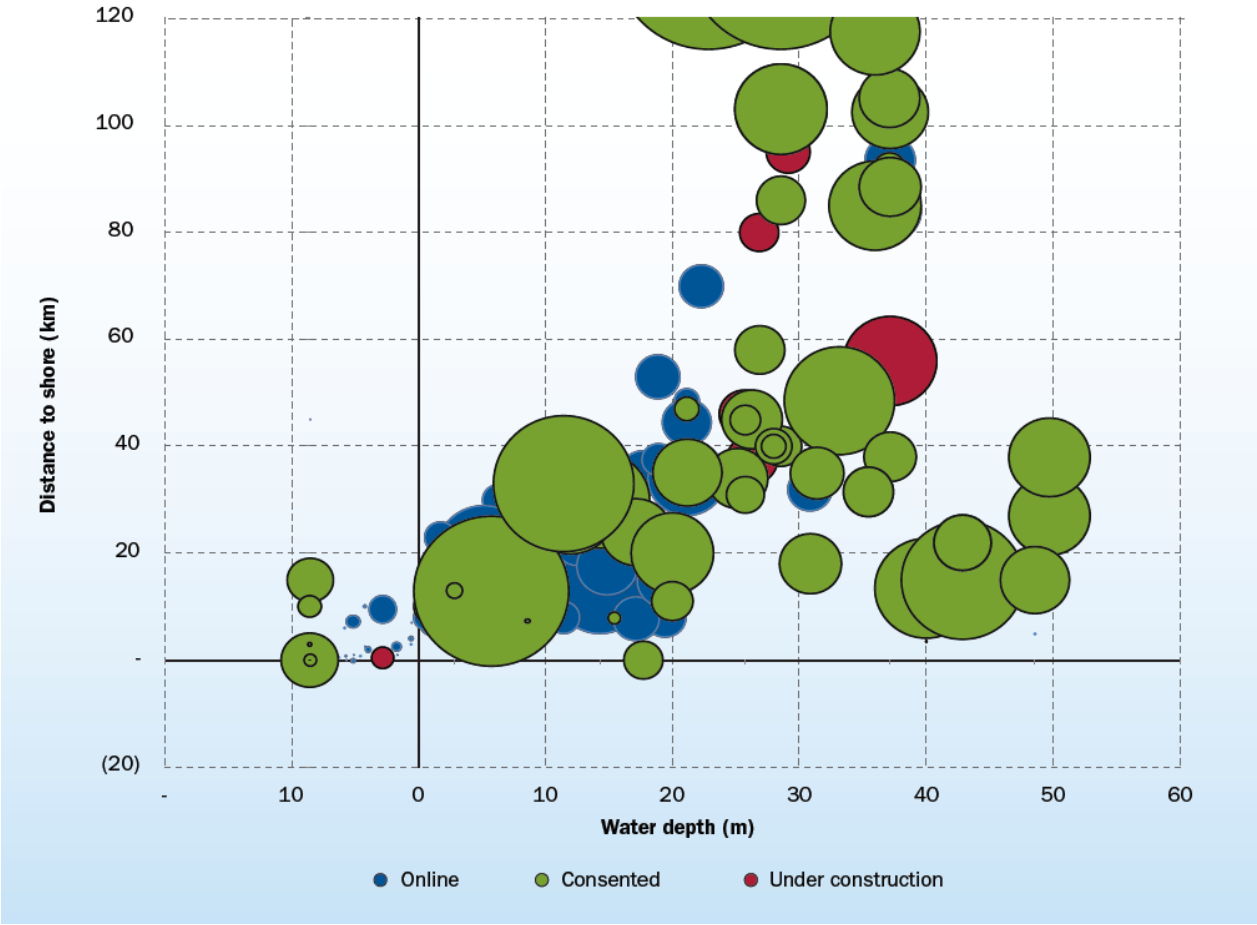

Figure 1.2: Average water depth and distance to shore of online, under construction and consented wind farms in Europe (EWEA, 2016)

top of the turbine, i.e. blades and nacelle, are jack-up vessels. This report is aimed to assess the pertinence of an uncommon type of vessel for top turbine installation, the floating crane vessel. The part of the turbine installation which is studied is the offshore mating of the blades on the rotor. The method detailed in this report for the blade installation is innovative and could lead to a redefinition of the current practices of the industry, thanks to the implementation of two unusual concepts, i.e. the use of a tower ring and a floating installation vessel. The tower ring concept is an innovative method proposed by De Groot (2015) that simplifies the mating of the blade on the rotor by the use of a frame and a ring attached to the blade and the tower respectively. Mating of the frame on the ring is made easier than a usual blade/rotor mating with bolts, and thus can be perform while the blade is lifted by vessel suffering wave-induced motions.

1.2 Objectives

This report focuess on the blade installation of bottom-fixed turbines with floating crane vessel. While jack-up vessels are commonly used for installing wind turbines by the industry nowadays, this report will be focused on the use of floating heavy lift vessels for lifting operations. This innovative method could allow a decrease of installing time because the time to put the legs of a jack-up vessel down is saved. While installing wind farms, the total installing time is mainly proportional to the time of installing one OWT. Thus, reducing the time of the installing method by a few hours can allow the installing company to greatly reduce costs and overall installing time. Calculations are conducted for environmental conditions of the North Sea, and for a specific floating vessel whose properties are described in Section 3.2. The turbine's properties and dimensions correspond to the DTU 10MW turbine. The detailed analysis of the installation is limited to the offshore mating of the blades on the turbine. Numerical analysis of the lifting and mating operation allows the establishment of the limiting sea states for performing the operation, and leads to a comparison of feasibility with jack-up vessel.

The main objectives of this Master's project are

1. To perform a state-of-the-art analysis of the top turbine installation practices for bottom-fixed turbines.
2. To establish the limiting sea states for blade installation using a floating vessel
3. To perform a weather-window analysis of the operation
4. To assess the feasibility of the floating vessel method and to compare it with the current jack-up vessel methods

1.3 Limitations

As the mating of the lifted blade on the turbine is the critical operation when installing blades, all the other sub-operations related to this installation are not numerically modeled. These operations include the installation of the frame on the blade, its lifting off from the vessel, its in-air displacement towards the mating location, and the rotation of the frame after installation on

the tower ring. The time needed to perform all these sub-operations is included in the operation feasibility assessment, but the limiting sea states used correspond to the mating of the frame on the tower ring. The resulting window analysis is conservative, as it is the case in most of marine operation studies. Another limitiation of this analysys is the nglecting of the impact of the guiding system of the tower ring during the connection with the frame. This leads to a certain degree of conservatism in the results, that can explain why the limitin sea states are narrow. Another cause of conservatism is the neglecting of the effect of passive or active motion compensation that are commonly used by floating installation vessel.

1.4 Organization

The rest of the report is organized as follows. The second section presents the state-of-the-art practices for top-turbine installation as well as an introduction to multi-body analysis and its implementation in the SIMA software used for the numerical analyses. The third section consists in the description of the lifting operation. This include the definition of the vessel chosen, the presentation of the tower ring concept and the description of configuration of the operation. The following section is focused on the representation of the aerodynamic loads acting on the lifted blade. Theory and implementation in the numerical model are included. In the fifth section, the results of the time domain and spectral analysis are included. A precise picture of the responses of the system to different sea state is showed. The sixth section consists in the establishment of allowing sea states, the weather window analysis and the comparison with Jack-up vessels. And finally, the conclusion of the reports and recommendations for future work are given.

Chapter 2

Introductive analyses

This chapter introduces the necessary knowledge about blade installation to follow the rest of the paper. A brief presentation of the theory behind multi-body analysis and its implementation in the software SIMO used for numerical computations is given.

2.1 State-of-the-art practices for blade installation

Unlike onshore wind turbine, there are many relevant concepts for designing the bottom part of offshore wind turbines (OWT). Turbines can be floating or bottom-fixed, and this paper considers only on the latter. Assembly concepts for the wind turbine are key points when designing offshore wind turbines, because they have a strong impact on the cost and the realization of the wind farm installation. Commonly, foundations of the turbines in the farm are installed first, and then tower, nacelle, rotor and blades are mated and connected to the foundation. There are different ways of designing turbine foundations depending on the water depth and the soil properties. For the method of connecting and installing turbine components on site, different choices are available depending of the degree of pre-assembling onshore. Another important aspect of the operation is the choice of the vessels used for transporting turbine components on site and for lifting them. The choice of the vessels will greatly impact the weather window and the operability of the overall installation procedure.

2.1.1 OWT foundations

A wind turbine is connected to the seabed thanks to a substructure and a foundation. The foundation fixes the substructure to the seabed, while the substructure is the interface between the seabed and the wind turbine. A transition piece is installed at the top of the substructure. It provides the connection between the substructure and the wind turbine and enables correction of any deviations from the vertical in the substructure. The transition piece assures that the wind turbine is installed perfectly vertically (Tveiten et al., 2015).

In the industry nowadays, there are 4 common categories of foundations: gravity-based, monopile, jacket, and tripod (see Figure 2.1). The choice of the turbine foundation, driven mainly by water depth, soil properties and cost, will impact the method for transporting it offshore, it can be wet-towed, towed on an external barge or transported by the lifting vessel. This choice will also impact the procedure for installing them on the seabed.

- *Gravity-based*: used preferably in waters with a maximum depth around 30 meters, are made of precast concrete and are ballasted with sand, gravel or stones.
- *Monopile*: used in water with a maximum depth around 25 meters. Made of steel, and driven into the seabed for about 30 meters with a hammer
- *Tripod*: used in deeper waters (up to 50 meters). Made of different pieces welded together and fixed to the ground with three steel piles.
- *Jacket*: used in deep waters (more than 40 meters). It is made of steel beams welded together, weighting more than 500 tons.

Above depths of 60 meters, bottom-fixed structures start to be less relevant than floating wind turbines, because of increased costs and bigger engineering challenges.

As shown in Figure 2.1, most of the current installed bottom fixed wind turbines are using monopiles. An important share is also using gravity based foundations. These trends are explained by the fact that monopile and gravity based are easier to produce, cheaper and simpler to install on site than the other foundation types. The turbine selected for the numerical study performed in this report has a monopile foundation. Three main factors are explaining this

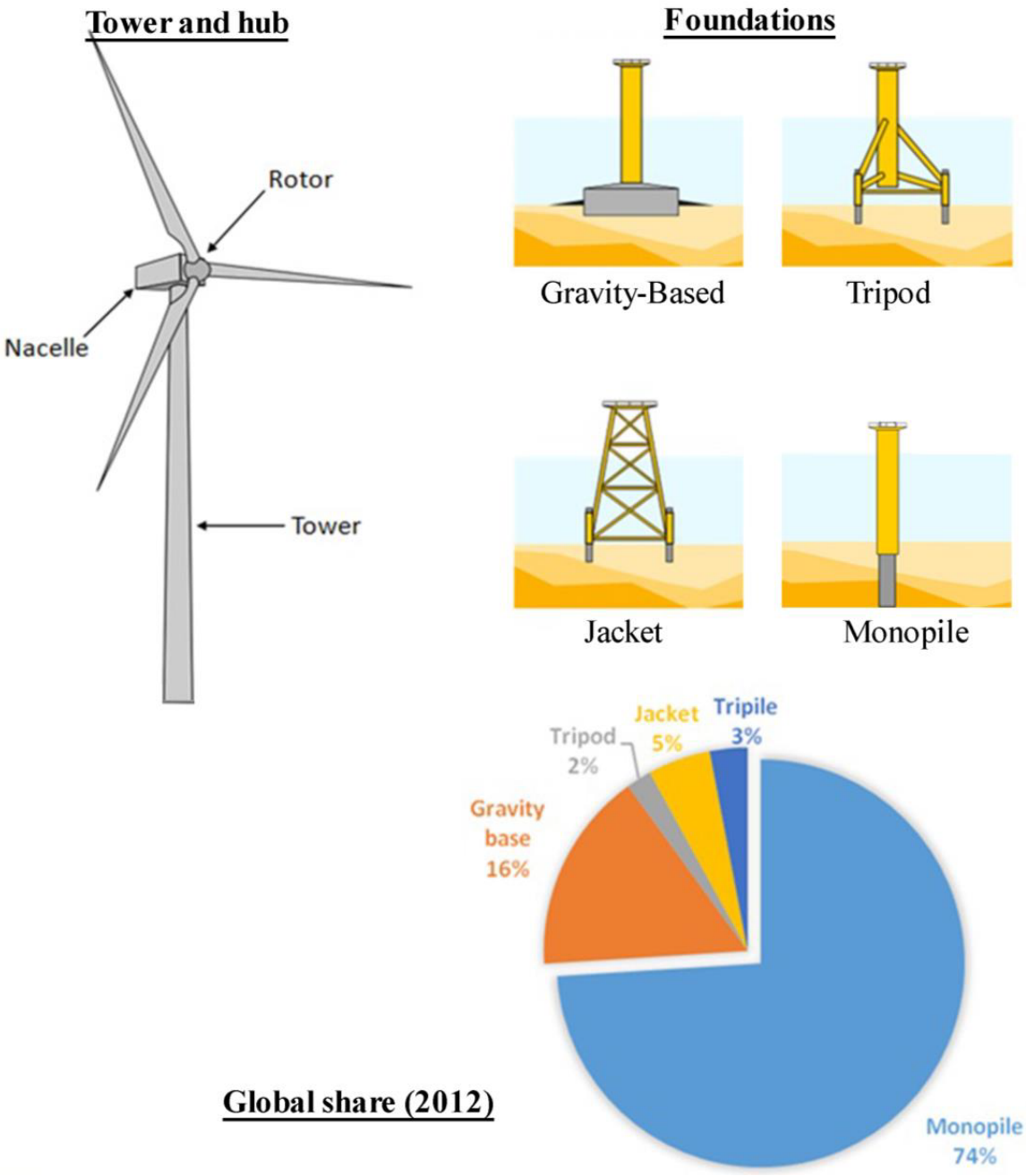

Figure 2.1: Main parts of an offshore wind turbine and typical fixed offshore foundations and their global share in 2012 - adapted from EWEA (2013) and Gawen (2014)

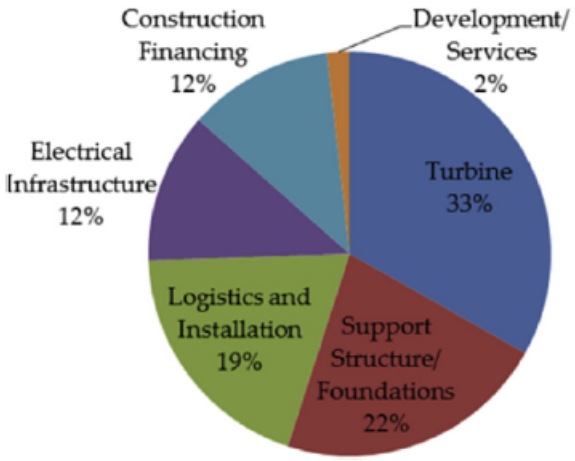

Figure 2.2: Offshore wind farm plant capital cost breakdown (Ahn et al., 2016)

choice. First, the industry has a high preference for this concept, making the study more relevant for most of the future wind farm installations. Secondly, it allows the installation vessel to come closer to the turbine since its footprint is minimal. Finally, assembly concepts based on OWT with monopile foundation are more likely to have some different level of offshore assembly.

2.1.2 Assembly concepts

Figure 2.2 shows that up to 20% of the total cost is spent for the installation, resulting in high priority for developing and designing efficient installation methods. Turbines with monopile foundations are usually installed in two or more times. First, all the monopiles are installed on site by hammering them into the ground. Then, the turbine is installed on top of the foundation, in one or more parts. These parts must be dry-towed on site by an external barge or by the installation vessel itself, and they are very sensitive to accelerations. Consequently, their transportation and installation are highly weather-sensitive.

Many different procedures can be implemented when installing OWTs. Mainly, these concepts differ in the degree of onshore preassembling, leading to different offshore installation steps. Solutions can vary from a full onshore assembly, leading to the transportation and installation on site of the total turbine in one piece, to a full offshore assembling, meaning that the turbine is transported as 7 elements (the two tower parts, the rotor, the nacelle and the three

blades) that are installed one by one on site (Uraz, 2011). Usually, wind turbine designers choose an intermediate solution that lies between these two extremes.

The lifting of the components at large heights (up to 100 meters for some turbines) requires really small motion of the lifting vessel, this is why mostly jack-up vessels have been used until now. It implies that turbine installation is very weather sensitive, and the associated weather windows force companies to favor summer period for farm installations. Such high lifts are also subjected to wind effects, reducing even more the acceptable environmental conditions.

The degree of onshore assembly will reduce the number of lifts performed offshore, and consequently impact the total operational time. However, assembled parts need more space on the deck of the lifting vessel or the external barges because of reduced efficiency in deck storage. It can lead to a higher number of trips from port to site, impacting also total operational time and reducing the interest for high degree of onshore assembly.

In this study, the assembly concept chosen is a partial offshore assembly. The concept is chosen from the work of De Groot (2015), based on a productivity study for the most feasible concept with floating vessel and tower ring concept (see Section 3.1). The OWTs have a high degree of onshore pre-assembly: the tower, nacelle, rotor and one blade are pre-assembled and transported on the deck of the installing vessel. Four OWTs are carried on deck and installed one after each other. The eight blades (two per OTW) are transported separately and installed at sea (see Figure 2.3). With this method, De Groot (2015) estimates the installation time to be 20 hours per OWT, including 4 hours per blade.

2.1.3 Installation vessels

As previously described, there are different kind of installation vessel relevant for OWT installation even though jack-up vessels are the common choice. Initially, the vessels used for OWT installation were vessels from the oil and gas industry, such as OSV. With the development of the wind offshore industry, some ship builders started to produce vessels that are more specifically designed for wind farm installation and maintenance. However, most of the vessels used nowadays are not vessels designed for wind farms. The main vessel types are (see Figure 2.4):

- *Jack-up vessel*: The vessel use a system of four legs that can be deployed until the seabed,

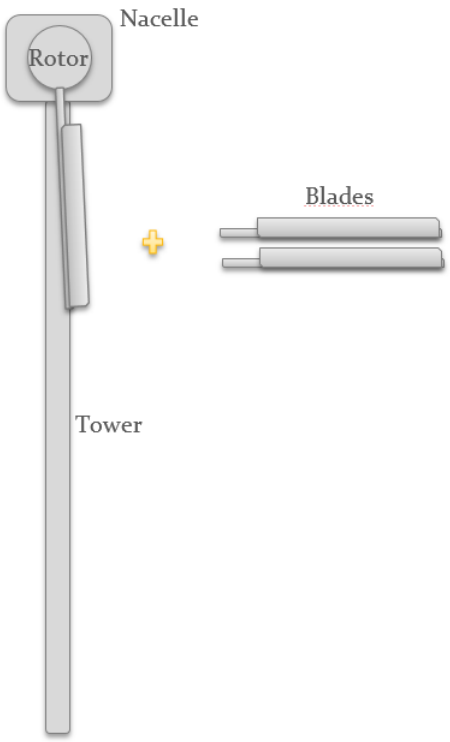

Figure 2.3: Assembly concept chosen

allowing the vessel to rise above the water level. The vessel is consequently free of wave-induced motions and can perform the lifting operation with optimal control.

- *Jack-up barge*: The concept is the same as for jack-up vessels, but they are not self-propulsed and thus, require to be towed to the site.

- *Crane barge*: This solution is relevant only when it comes to the installation of totally pre-assembled OWTs. However, it rises a lot of challenges such as towing the barge to site and deploying the mooring lines and is therefore often disregarded in comparison to jack-up solutions by the industry.

- *Floating installation vessel*: It includes two specific vessel design. The Offshore Supply Vessel (OSV) and the Wind Turbine Installation Vessel (WTIV). The latter ones are designed specifically for the offshore wind industry, while the OSVs have a more generic use. They are monohull heavy lift vessels, with dynamic positioning (DP) and mooring lines.

The main objective of this thesis is to assess the feasibility of the floating installation vessels when it comes to blade installation, instead of the currently used jack-up vessels.

2.1.4 Blade mating

For the assessment of the feasibility of the selected operation, this paper follows the guidelines of Acero et al. (2016). This method, of which a brief description is given in Section 6.1, is based on the determination of critical events of each sub-operation and their numerical modeling. Results from the simulation based on these models allows the operation designer to establish the limiting environmental conditions.

The critical operation when it comes to blade installation is the mating of the lifted blade in the rotor. This operation is performed at great heights (circa 100 meters) and needs extreme precision. As shown in Figure 2.5, each of the multiple bolts of the blade must be mated simultaneously into the conic holes of the rotor. Blade are mated one by one, and the most common configuration is to mate them horizontally. Some tug lines are usually deployed to reduce the in-air motions. The ideal configuration has been the focus of several studies, since it has an important impact on the external forces and induced motions. Kuijken (2015) has been working on

Figure 2.4: Vessels used for OWT installation. From top left, clockwise: Artist view of the Mir-Tac's Jack-up barge (Picture: offshorewind.biz), Crane barge (Picture: Scaldis), DP crane vessel Swiber Kaizen 4000 (Picture: thrustmaster.net) and Wind Turbine Installation Vessel Pacific Orca (Picture: worldmaritimenews.com)

Figure 2.5: Mating of a blade on the rotor (from SeajacksUK Youtube Channel www.youtube.com/channel/UCpSMVnU3NyoTtQbhU73dU3w)

aerodynamic modeling of the lifting of blades, depending on the configuration of installation. It results that 45° of pitch for the blade must be avoided, and that the most appropriate pitch angle is 90°.

His recommendations are not followed here, because this report is based on the introductive work of De Groot (2015). The introduction of the tower ring reduces the accuracy needed when mating the lifted blade and its frame on the OWT. It results in important consequences for the bolt mating process. First, it is not anymore the critical event because it is performed when the blade frame is already fixed to the tower and consequently the wind- and wave-induced motions of the frame are almost null. The critical event is the mating of the frame on the tower ring. Secondly, the bolt mating is done almost vertically, and not horizontally as it is usually performed.

2.2 Multi-body analysis

The analyses performed in this report consist in solving a multi-body problem with coupled interactions and integration of hydrodynamic and aerodynamic loads.

The vessel is subjected to hydrodynamic loads, based on the potential flow theory (MARIN-

TEK, 2015a). The radiation and the diffraction problem are solved, and the Morison's equation for quadratic viscous drag is applied on the vessel as it is considered a large volume structure (Zhao et al., 2017). 2nd order wave loads are also taken into account by the use of the 2nd order potential flow theory. Aerodynamic loads acting on the vessel are neglected since they are very small compared to the hydrodynamic ones.

The lifted object is considered as a large volume hanging in air, and is consequently subjected to aerodynamic loads. The formulation of these loads is performed by an external code and is explained in Chapter 4.

Several coupling lines connect the vessel, the hook and the lifted object (see Section 3.3) . It creates a coupling between the equation of motions of the different bodies.

Finally, the dynamics of the multi-body system is derived from Equation 2.1 (Zhao et al. (2017) and MARINTEK (2015a)).

$$\left[(M + A(\infty)\right]\ddot{x} + D_1\dot{x} + D_2 f(\dot{x}) + Kx + \int_0^t h(t-\tau)\dot{x}(\tau)d\tau = F(t,x,\dot{x}) \tag{2.1}$$

where,

- M is the total mass matrix for the vessel, hook and lifted body;
- x is the rigid body motion vector with 15 DOFs (6 for the vessel, 3 for the hook and 6 for the lifted body);
- A(∞) is the added mass matrix at infi

  nity frequency;
- D_1 is the linear damping matrix;
- D_2 is the quadratic damping matrix;
- K is the coupled stiffness matrix;
- h is the retardation function of the vessel which includes both the frequency-dependent added mass and damping;

- F is the external force vector that includes the aerodynamic loads and the hydrodynamic loads.

The coupled stiffness matrix includes both the hydrostatic stiffness of the vessel with the impact of mooring lines, and the system stiffnesses due to the mechanical couplings between bodies. These couplings are linear and their stiffnesses have two components: the elasticity stiffness and the connection flexibility (Zhao et al., 2017).

For the analysis purposes, the natural frequencies of the system must be determined. Solving the Equation 2.2 (Zhao et al., 2017) gives the natural frequencies and their associated modes.

$$\left[-\omega^2(M+A)+K\right].X = 0 \tag{2.2}$$

2.3 SIMO software

SIMO stands for SImulation of Marine Operations and is a computer program for simulation of motions and station-keeping behavior of a complex system of floating vessels and suspended loads (MARINTEK, 2015b). Essential features are:

- Flexible modeling of multi-body systems
- Non-linear time domain simulation of wave-frequency as well as low-frequency forces
- Environmental forces due to wind, waves and current
- Passive and active control forces
- Interactive or batch simulation

SIMO is developed by MARINTEK and is part of SIMA, a powerful tool for modeling and analysis of tasks within the field of marine technology. The main features of SIMA are SIMO, RIFLEX, and the coupled SIMO-RIFLEX.

The main theory exposed in the previous section is implemented in the SIMO software, which form a comprehensive aero-hydro-mechanical simulation tool. The aerodynamic calculations of SIMO are limited when it comes to the modeling of aerodynamic behavior of a lifted

blade, so an external code is introduced (see Chapter 4) to perform the required computations. At each time step, SIMO computes the hydrodynamic loads and coupling forces, and communicates the lifted body motions to the external tool. The tool computes the aerodynamic loads and communicate them back to SIMO to be integrated in the equations of motion of the system as external forces. These equations of motions are then solved and the software goes onto to the next time step.

Chapter 3

Description of the operation

This chapter gives a description of the concepts chosen for the simulation models. The tower ring concept from De Groot (2015) is briefly described and the characteristics of the installation vessel. The last sub-section gives an overview of the configuration of the operation.

3.1 The tower ring concept

The tower ring concept is described as an extra system installed on the tower that is used to connect the blade to the tower in order to remove the parasite movements due to waves and wind during lifting operations. This innovative design is introduced by De Groot (2015) in his thesis for TU DELFT and the company Seaway Heavy Lifting. After having performed a feasibility study focused on time- and cost-saving innovative methods that could replace jack-up installations, De Groot concludes that the introduction of the tower ring concept could reduce by half the installation time of an OWT. Scaled to a full offshore wind farm installation, this could results in substantial cost savings for the deploying companies.

In the following section, a brief description of this concept is given for the reader's comprehension. More detailed information can be found in the thesis of De Groot (2015).

The concept of the tower ring installation method is represented in the Figure 3.2. In comparison to the traditional horizontal bolt mating, two systems for facilitating the blade installation are introduced: the tower ring and the blade frame (see Figure 3.1). First, a tower ring is attached to the tower. Then, on deck, the blade is mounted on the frame. The frame holds the

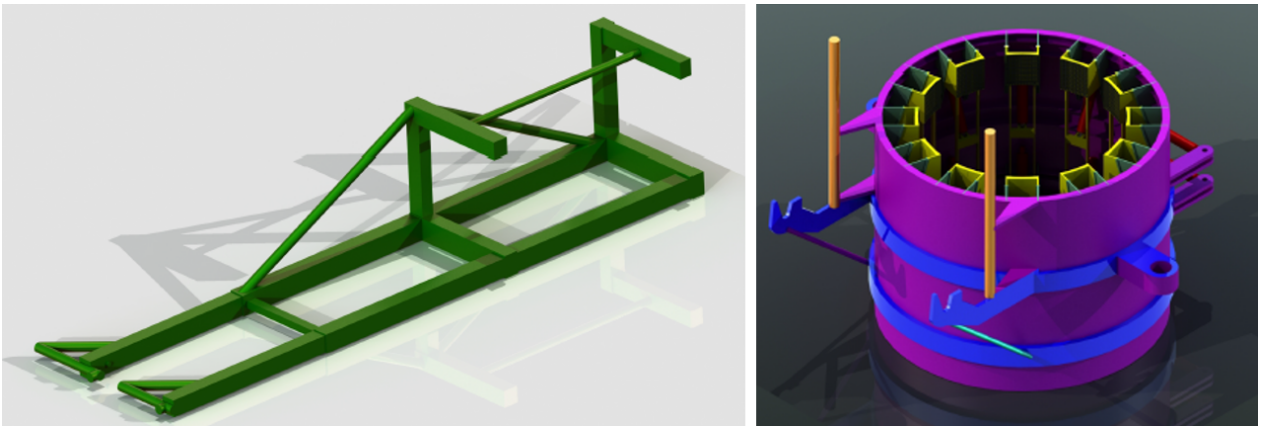

Figure 3.1: Blade frame (left) and tower ring (right) (De Groot, 2015)

blade and is lifted onto position by the crane of the vessel. Ring and frame are mated before the connection of the rotor and the blade is realized. The mating is done by connecting the hanging points at the end of each beam of the frame on the two hooks located on two external arms of the ring. Guides and bumpers are designed to help reducing the frame motion while the connection is realized. Once frame and ring are connected, the frame is rotated downwards and the telescoping arms are shortened, until blade bolts connect with the rotor.

This system allows the blade lifting frame to be connected to the tower during mating of the bolts. It eliminates the wave and wind induced motions that every object lifted by a floating installation vessel is subjected to. However, it moves the problem of lifting motions from mating the bolts to mating the blade frame on the tower ring concept. This operation is easier to realize than the traditional horizontal mating concept and need less accuracy, as explained in section 6.1. It could consequently be seen as a big step towards the use of floating installation vessel when installing offshore wind farms.

More information about the frame geometry and dimensions are given in Appendix B.

3.2 Description of the vessel

To obtain consistent results, the vessel characteristics used in the numerical models must be based on a realistic vessel. Some of the main characteristics of the vessel are described in this section (see Table 3.1 and Table 3.1), and more information can be found in Appendix B. The choice of the vessel was driven by the selection of a heavy lift vessel capable of lifting heavy

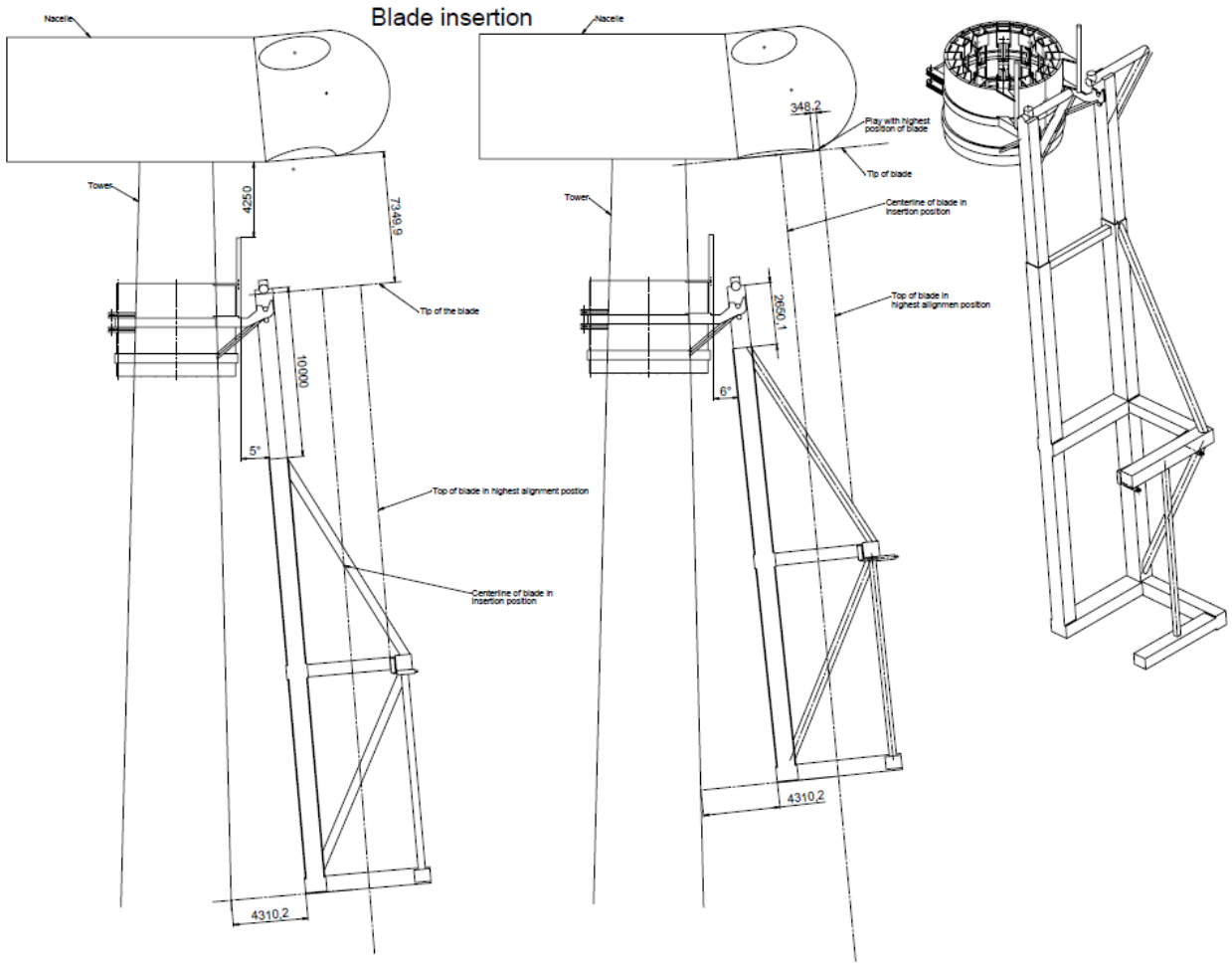

Figure 3.2: Technical drawings of the blade mating with tower ring concept (De Groot, 2015) (Drawn on Solidworks)

Figure 3.3: Oleg Strashnov, a vessel with similar properties as the one used in the report (Picture: MarineTraffic.com)

objects (400 tons if lifting together nacelle, rotor and a blade) up to 110 meters high for top turbine installation purposes.

The chosen vessel is a monohull heavy lift floating crane vessel (see in Figure 3.3 a picture of a similar vessel). She is 183m long, 47m wide and has a 12m draft. The crane is capable of performing lifts of up to 5000 tons at an outreach of 32 m in fully revolving mode. The main hook featured a clear height to the main deck of the vessel of maximum 100m. The vessel is designed with a combination dynamic positioning system and eight catenary mooring line system. The positioning system allows the vessel to operate in shallow water and in close proximity with other structures. Therefore, the lifting capacity and the positioning system of the floating vessel make it capable of performing the installation of monopiles or jackets in shallow-water sites as well as turbine tower and top turbine.

Her deck space is around 3 700 squared meters, and the vessel is designed for multi-operation purposes, such as upending of jackets, heavy structures installation, and TLP/SPAR deployment.

Table 3.1: Main characteristics of the vessel

Length [m]	183
Width [m]	47
Draft [m]	12
Lift capacity [tons]	5000
Lift Outreach [m]	32
Deck space [m²]	3700
Transit speed [knot]	14

Table 3.2: Mass coefficient and mass moments of inertia about origin

Mass [kg]	I_{xx} [kg.m²]	I_{xy} [kg.m²]	I_{yy} [kg.m²]	I_{zx} [kg.m²]	I_{zx} [kg.m²]	I_{zz} [kg.m²]
6.3452e+07	2.827 e+10	0	1.501 e+11	0	0	1.501 e+11

Outfitted with state-of-the-art technologies, the vessel has a transit speed of 14 knots and is designed for oil and gas industry as well as for external marine activities, wind farm installation for example.

3.3 Operation configuration

To perform the blade installation operation, the vessel is positioned close to the tower and maintained in position with the help of its eight mooring lines and the dynamic positioning system. As it is shown in Section 5.2, the roll motion of the vessel has a high impact on the motion of the lifted blade. Therefore, the vessel is located preferentially parallel to the waves' main direction to minimize roll motions. The blade is set perpendicular to the vessel orientation and hanging on the right side of the vessel. The blade is hung in the air by the corners of the top braces of the frame. The setup of the operation is depicted on Figure 3.6 and Figure 3.7 from top view.

The lifting system is composed of a hook connected to the frame by four slings. The hook is considered as an individual body with a mass of 10 tons. To reduce motions of the lifted blade and frame system, two tug lines are deployed from the crane boom. They are defined as two parallel short lines fixed to the frame at the bottom corners between the beam B and the vertical beams D and G respectively (see figure**??**) and an initial pre-tension of around 50kN on each line is applied. This lifting system brings an angle between the lifting wire and the vertical axis (see Figure 3.7), allowing the avoidance of stack in the lines. The properties of the lifting wire,

Figure 3.4: Artist view of the operation configuration (adapted from www.MarineTraffic.com and De Groot (2015))

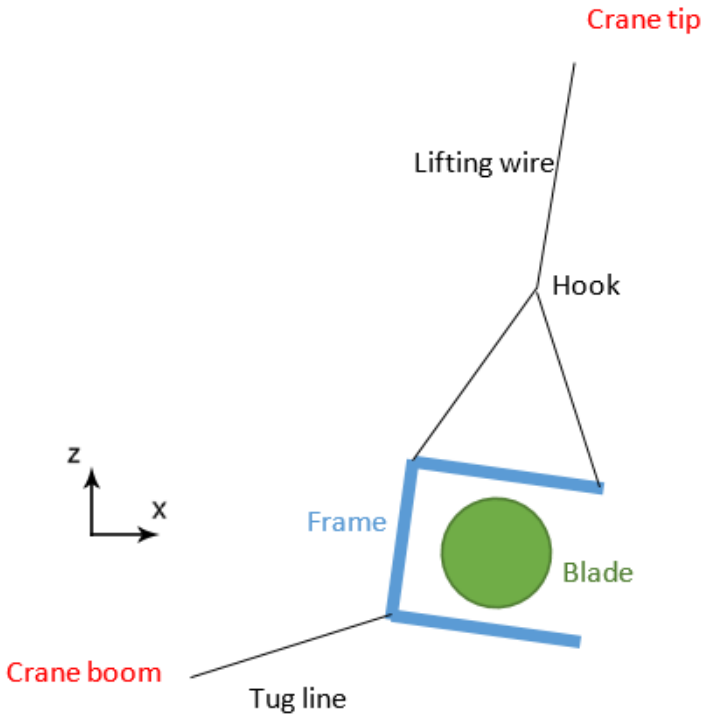

Figure 3.5: Lifting system - Side view

slings and tug lines are described in Table 3.4. They are set perpendicular to the frame, in order to have a better impact on wind forces cancellation. For this matter, the vessel must be located preferentially parallel to the main direction of the wind. The OWT properties and dimensions of this study are based on the DTU 10 MW turbine which is aimed for research purposes. Some important characteristics of the turbine are given in Appendix B.

Here, a problem rises: the best configuration for the vessel appears to be parallel to both the wind and the waves main direction. Even though this particular environmental condition is not rare, a lot of other environmental configurations are possible. The analyses performed in this paper are considering three different set-ups for wind and wave directions. A better picture of the ideal configuration is given and it also shows the impacts of the less ideal ones on the feasibility of the operation.

The three environmental conditions are the following (see Figure 3.8):

- No angle between the mean wind and wave directions (noted as 0_0)
- 30° angle between the mean wind and wave directions (noted as -15_15)

Table 3.3: Location of points of interests of the vessel

Location	x[m]	y[m]	z[m]
Center of gravity	-7.593	0	1.983
Crane bottom	-74.2	0	10
Crane tip	-20	-32	137
Tug line 1 fixing point	-30	-26	108.38
Tug line 1 fixing point	-30	-38	108.38

Table 3.4: Wire and line properties

Wire	Length [m]	Flexibility [m/N]	Damping [N.s]	EA [N]
Lifting wire	5.02	2.0 e-07	5.0 e+06	5.0e+08
Lifting slings	18.833	0.0	1.25e+06	1.25e+08
Tug lines	5.0	0.0	35000	3.5e+06

- 60° angle between the mean wind and wave directions (noted as -30_30)

In the first case, the wind and the waves are coming from the stern of the vessel. It means that the vessel is not facing them, but oriented towards the outflow direction. This set-up is chosen because it allows the tug lines coming from the crane boom to have a tension opposite to the mean component of the wind forces. This configuration maximizes their effectiveness.

In the second case, the vessel is located to have equal angles between its main axis and the two wind and wave directions. These angles are -15° and 15° respectively. This choice is explained by the need to minimize both angles in order to limit the blade and frame motions. As in the first case, the vessel is facing the outflow direction.

The third case has the same set-up as the second one, but angles are now -30° and 30°.

In all the cases, the wave distribution is defined by the JONSWAP spectrum with two key parameters being the significant wave height and the peak period. The turbulent wind model is the IEC Kaimal Model (IEC, 2005). The IEC standard selected is 61400-3, with turbulence characteristic C.

3.4 SIMO modeling

During the modeling of the operation in SIMO, multiple decisions had been taken to simplify the reality. In this section, the modeling decisions and hypotheses taken are described.

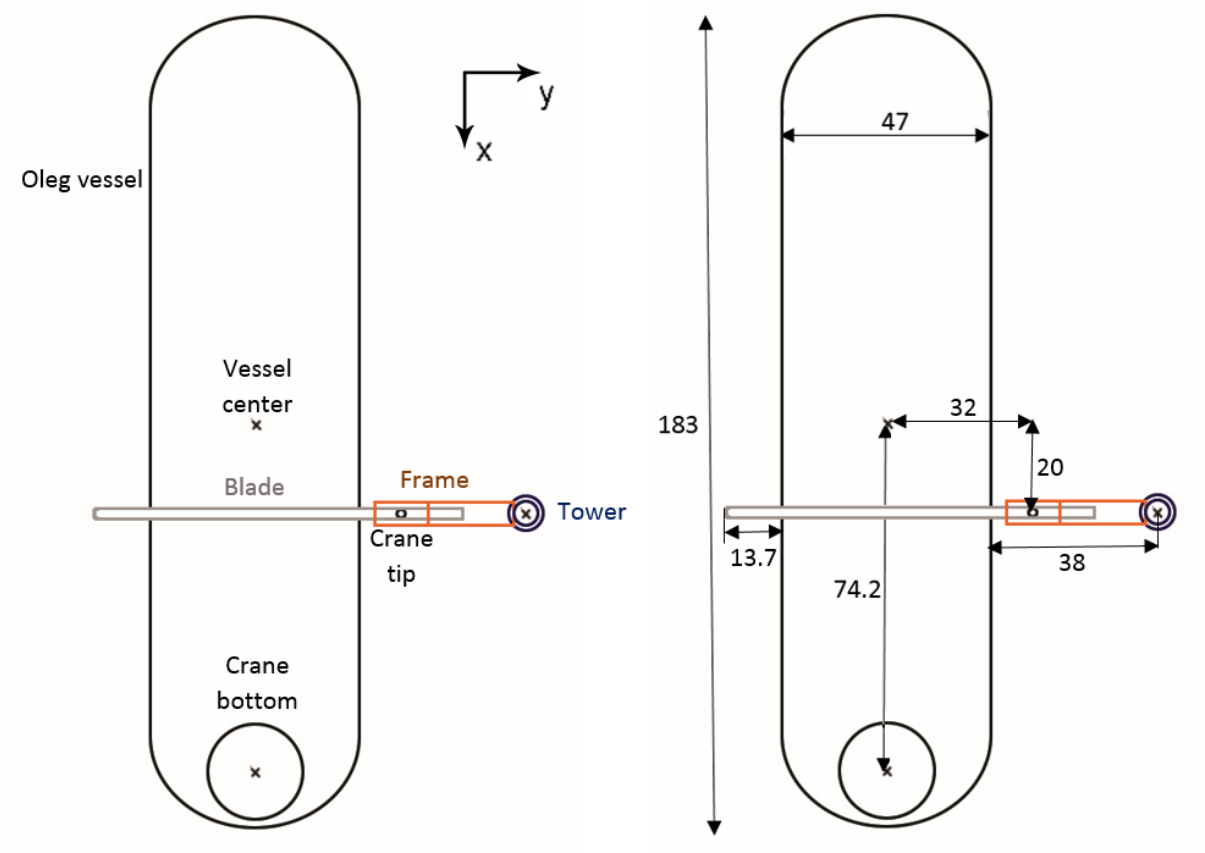

Figure 3.6: Schematic drawing of the operation configuration - Top view

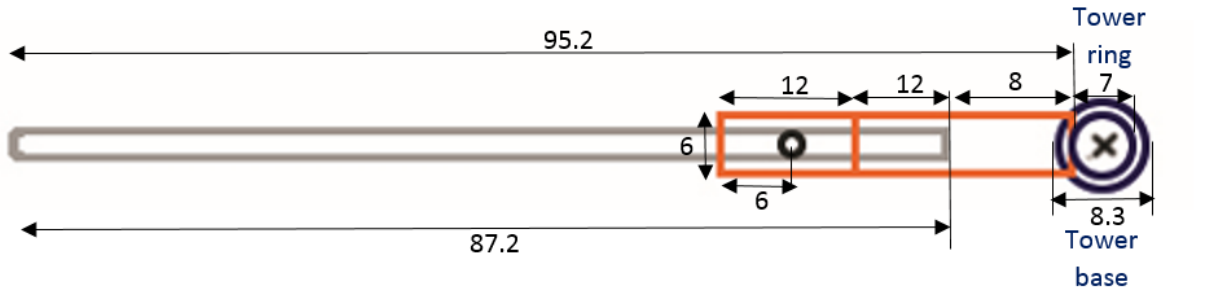

Figure 3.7: Schematic drawing of the blade and tower configuration - Top view

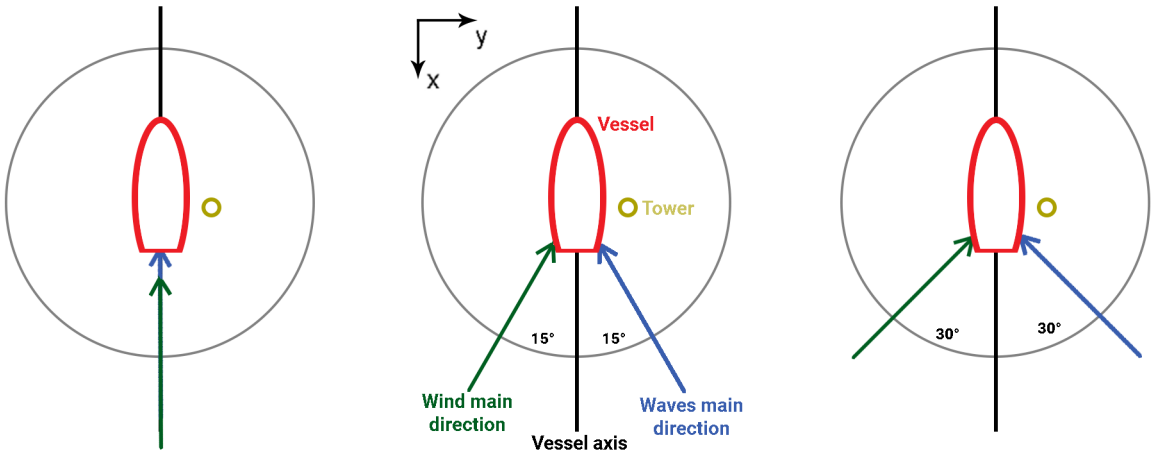

Figure 3.8: Top view of the three environmental cases studied depending on the angle between mean wind and waves direction. From left to right: case 1 with 0°, case 2 with 30° and case 3 with 60°.

First, the operation is considered as a three body analysis: the vessel, the hook and the blade and frame system. Blade and frame are supposed to be rigidly connected, which is not totally the case in reality. However, the impact of the small variation in position that the blade can suffer when connected to the frame are neglectable, as it is shown by De Groot (2015). The wires are considered as weightless, which is relevant when compared to the high weight of the other bodies considered. Figure 3.9 shows a 3D representation of the operation from the SIMO model. The reference frame in the SIMO is the one depicted on the figure: origin located at the center of the vessel at sea level height, x axis along the main vessel axis, from stern to bown, y axis from starboard to port side, and z axis vertical, pointing upwards. This system of coordinates is the one used in the results.

A second assumption is made, regarding the rigidity of the blade and frame body. The structural elasticity of these lifted bodies are assumed to have small impacts on the aerodynamic loads, as it is shown by Gaunaa et al. (2014). Consequently, the blade and frame body is considered as a single rigid body for the SIMO and the aerodynamic computations.

Another modeling simplification is to assume that the lifting wire cable has a constant length during the operation. In reality, it is elongated and shortened while the vessel crew proceeds to the installation, but the variations are slow and their impact is therefore considered as neglectable.

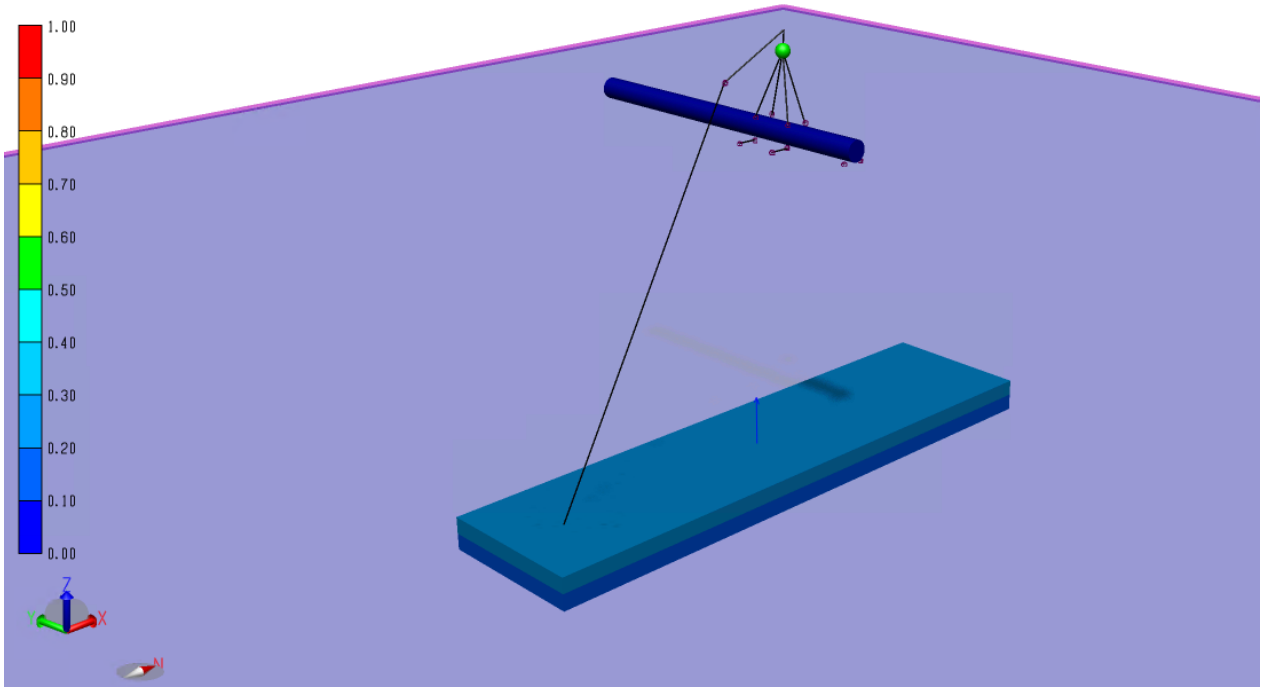

Figure 3.9: 3D modeling of the multi-body problem in SIMO

As explained in Section 6.1, the hanging system introduced by the ring and the frame is helped by guides and bumpers. The impact of these guides and bumpers is signifcant to reduce the motions of the lifted blade, but they are not modeled in SIMO. This leads to a conservative analysis, as it is often done in marine operation analyses. The blade is consequently modeled in-air, without any modeling of the OWT, its tower or the ring. The results are focused on frame tip motions, and their interpretation will be sufficient to determine the feasibility of the operation.

One of the modeling issue is the implementation of turbulent wind loads on the lifted object. The models for wind loads present in the core software of SIMO are not appropriate to meet the requirements of this analysis. During mating of the blade, the impact of the wind turbulence is not neglectable and must be considered. An external tool interacting with the SIMO computations at each time step is required. This tool is described in the following chapter.

The reference frame of SIMO is depicted in figure 3.9. The origin is located at the center of the vessel, on the sea surface plane. The x-axis is directed along the main axis of the vessel, from stern to bow. The y-axis is also horizontally located, and is directed from starboard to port side of the vessel. The z-axis is vertical and pointing upwards.

Chapter 4

Aerodynamic loads on the lifted blade

This chapter presents the modeling of the wind loads acting on the lifted blade and frame body. An external code is implemented in the SIMO computations to depict accurately the behavior of the blade and frame while subjected to important wind forces. This external code comes from the work of Zhao et al. (2017) and Cheng et al. (2016) to provide integrated simulation tools for aerodynamic calculations in SIMO, called SIMO-Aero and SIMO-Riflex-AC, respectively. While these codes were used for the implementation of wind loads on a lifted blade with various roll, pitch and yaw angles, the code used for this paper's analyses is adapted to consider also the impact of the loads acting on the frame.

4.1 Theory

The theory of the aerodynamic load calculation presented in this section is based on the cross-flow principle and its interpretation by Zhao et al. (2017) for the calculation of a lifted blade. In the work of Zhao et al. (2017), the lifted wind turbine blade is considered to have a local blade shape that suits a 2D approximation. The linear discretization of the blade and the application of the cross-flow principle allows the simplification of the calculation of aerodynamic loads into multiple 2D computation of lift and drag forces (see Figure 4.1). Indeed, the spanwise flow velocity is neglected, and thus the flow velocity can be expressed in the plane of the cross-section of each blade element. The global inflow velocity is calculated as the subtraction of the free wind velocity by the blade element local velocity. The induced velocity by blade motion is here

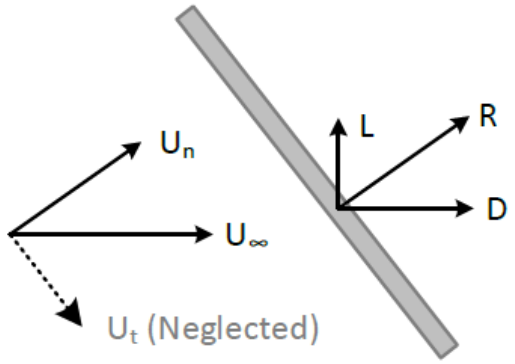

Figure 4.1: Illustration of cross flow principle (Zhao et al., 2017)

neglected (Zhao et al., 2017). From the global inflow velocity, the angle of attack is determined. Drag and lift coefficients can then be found by using look-up tables based on the angle of attack. Finally, drag and lift forces and moments are computed along the blade and expressed at the blade center.

For this calculation, the need to introduce the frame as a body subjected to aerodynamic loads forces us to modify the external code. As for the blade, the frame must be discretized in elements. All the steps performed for the aerodynamic calculation of the loads acting on the blade are kept, except that the final computation of the drag and lift loads is now also taking into account the ones acting on the frame elements. However, some differences occur for the frame elements load computation. First, we assume that there is no transverse loads or displacements due to the wind action on the frame. Consequently, we neglect lift forces and all transverse vibrations of beams. This can be explained by the shape of the beams composing the frame structure. Being rectangular or circular, the transverse effects from the wind are very small in comparison to the longitudinal ones. Secondly, the frame elements have various orientations due to the presence of vertical and horizontal beams in the structure. Thus there is the need for a definition of an orientation basis for every element.

With the introduction of the frame, the question of the shield effect rises. The incoming flow on some elements is disturbed from the upstream beams or blade part. Towards this problem, another assumption is made: no shield effect is taken into account from one element to another. Consequently, we suppose that elements are distant enough from one to another to neglect the perturbation in the flow from elements upward in the wind direction. This results in, for exam-

ple, having drag forces acting on beams A and B even when wind is coming in the x direction and A is being behind B (see Figure B.2).

For the implementation of this aerodynamic load calculation in SIMO, an external code communicating with the software must be implemented. At each time step t, the aerodynamic loads are expressed as external force and moment acting on the center of the blade and frame body. The next section describes step by step the code computations for the expression of aerodynamic loads acting on the frame. The blade load step by step procedure is not described here since it is already explained by Zhao et al. (2017).

4.2 Numerical implementation in SIMO

The following procedure is explaining how the drag force is computed for each element at each time step. Once the drag forces acting on all the elements are computed and expressed in the global coordinates, the resulting aerodynamic global force and moment are computed at the center of the Blade+Frame body and then transferred to SIMO. These resulting loads are computed by considering also the forces on blade elements, but this procedure is not described here.

The procedure for aerodynamic calculation is described in the following sections. It is also depicted in Figure 4.2 by a schematic flow chart.

4.2.1 Definition of the reference bases

For the problem considered, due to the formulation of parameters in SIMO and the way of calculation of aerodynamic forces, the coordinates of vectors can be given in three different bases (see Figure 4.3). These bases are:

- The reference basis ϵ (O, x,y,z), which is fixed and the original basis from where the position of the vessel and the hanging blade are defined. It is also the coordinate system of reference in SIMO.

- The blade+frame basis B (O_b, x_b, y_b, z_b), which is located at the center of gravity O_b of the blade, where x_b points towards the spanwise direction of the blade, y_b follows the ax-

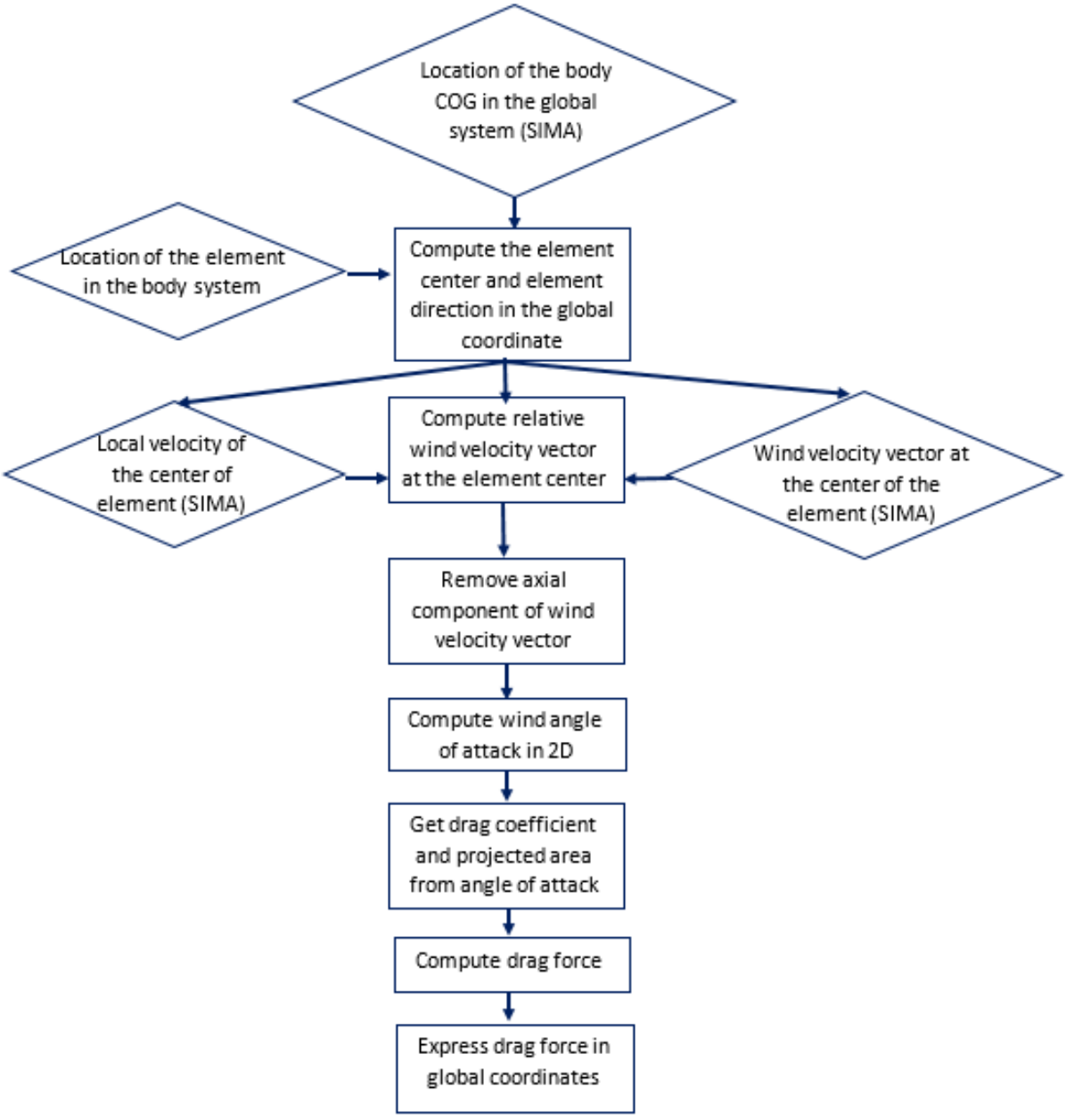

Figure 4.2: Flow chart for aerodynamic calculation on one element

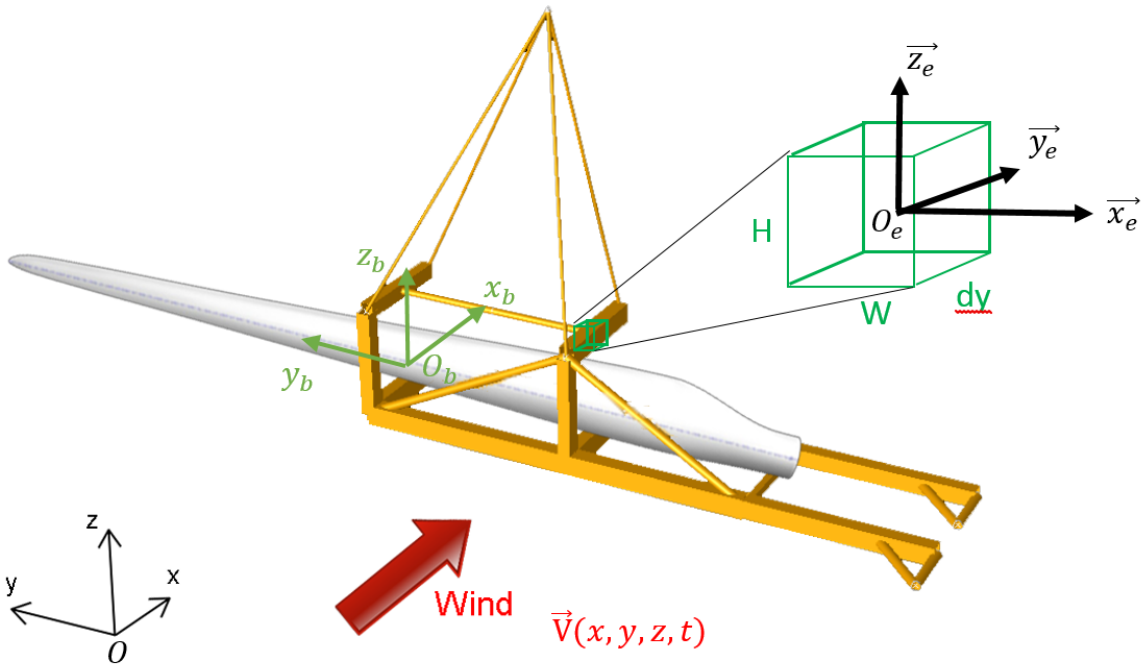

Figure 4.3: Definition of the coordinate system - Adapted from De Groot (2015)

ial direction of the blade, pointing toward the blade tip, and z_b is orthogonal to the two precedent axis, meaning it is pointing in the vertical direction of the frame.

- The element basis E (O_e, x_e, y_e, z_e), is located at the center O_e of the beam element considered, where x_e is directed along the width of the element, y_e along its length and z_e along its height.

We need to establish the matrix of change of basis. The matrix of change of basis from basis B to basis B' is defined as the matrix verifying the Equation 4.1.

$$V_B = P_{BB'} V_{B'} \tag{4.1}$$

With V_B the vector V expressed in the basis B and $V_{B'}$ the vector V expressed in the basis B'. It is important to note that, because B and B' are orthogonal bases, the inverse of $P_{BB'}$ is ${}^tP_{BB'}$.

If the transformation to obtain the basis B' from the basis B is a unique rotation θ around the axis x of the basis, the matrix of change of basis $P_{BB'}$ has the form described in Equation 4.2.

$$P_{BB'} = \begin{bmatrix} 1 & 0 & 0 \\ 0 & cos(\theta) & -sin(\theta) \\ 0 & sin(\theta) & cos(\theta) \end{bmatrix} \tag{4.2}$$

In the aerodynamic calculations, the matrix of change of basis P_{BE} from B to E is not dependent of time since the blade+frame body is considered as rigid. It is different for every element depending on its position along the frame. The definitions of this basis is calculated for every element from the discretization of the frame (see AppendixB)

However, the matrix $P_{\epsilon B}$ of change of basis from ϵ to B is dependent of time since the blade+frame body and its related axis are moving. To know the relation between the axis of these bases, the current rotations of the B+F body at the time step considered need to be extracted from SIMA. These rotations are X_L, Y_L and Z_L, rotations along the x, y and z axis respectively. In the case of small rotational angles, we can neglect the second order effect and act as if the rotations was be independent from each other, but in our case, we cannot neglect it since the B+F body may experience large rotational displacements. The order of application of these rotations is given in SIMA by:

$$Z_L \longrightarrow Y_L \longrightarrow X_L$$

We can decompose the change of basis from ϵ to B in three steps, one rotation at a time. After having applied the three rotations, the expression for the matrix $P_{\epsilon B}$ is described in Equation 4.3.

$$P_{\epsilon B} = \begin{bmatrix} cos(Y_L)cos(Z_L) & cos(Z_L)sin(X_L)sin(Y_L) - cos(X_L)sin(Z_L) & sin(X_L)sin(Z_L) + cos(X_L)cos(Z_L)sin(Y_L) \\ cos(Y_L)sin(Z_L) & cos(X_L)cos(Z_L) + sin(X_L)sin(Y_L)sin(Z_L) & cos(X_L)sin(Y_L)sin(Z_L) - cos(Z_L)sin(X_L) \\ -sin(Y_L) & cos(Y_L)sin(X_L) & cos(X_L)cos(Y_L)) \end{bmatrix} \tag{4.3}$$

4.2.2 Location of element center

The location of the center of gravity O_b in the reference basis ϵ is extracted from SIMA and varies at every time step:

$$\overrightarrow{OO_b} = \begin{bmatrix} X_G \\ Y_G \\ Z_G \end{bmatrix}_E \tag{4.4}$$

The location of the beam element center in the B+F basis B is independent of time and known as:

$$\overrightarrow{O_bO_e} = \begin{bmatrix} X_E \\ Y_E \\ Z_E \end{bmatrix}_B \tag{4.5}$$

Then the location of the beam element center in the reference basis ϵ is described by the relation:

$$\overrightarrow{OO_e} = \begin{bmatrix} X_G \\ Y_G \\ Z_G \end{bmatrix}_E + P_{\epsilon B} \begin{bmatrix} X_E \\ Y_E \\ Z_E \end{bmatrix}_B \tag{4.6}$$

$$= \begin{bmatrix} X_OE \\ Y_OE \\ Z_OE \end{bmatrix}_E \tag{4.7}$$

4.2.3 Wind velocity vector at the center of the element

The turbulent wind is produced by a wind grid moving spatially through time. The wind data is stored in a binary file. When extracting the data from the file, the total wind field with its three axial components in the reference basis ϵ at every time step and every spatial increment is known:

$$V_{W\epsilon}(x,y,z,t) = \begin{bmatrix} V_{W\epsilon x}(x,y,z,t) \\ V_{W\epsilon y}(x,y,z,t) \\ V_{W\epsilon z}(x,y,z,t) \end{bmatrix}_\epsilon \tag{4.8}$$

Linear interpolation between the wind vectors at the closest spatial incremental points of

the grid from the beam element center is required to get the value of $V_{W\epsilon}(X_{OE}, Y_{OE}, Z_{OE}, t)$. This vector will simply be noted $V_{w\epsilon}$ for the rest of the report. It needs to be expressed in the element basis E:

$$V_{wE} = P_{EB} P_{B\epsilon} V_{w\epsilon} \tag{4.9}$$

4.2.4 Calculation of relative velocity of the element

From SIMA, we get the local velocity for the 6 degrees of freedom of the center of gravity O_b of the B+F body at every time step. This local velocity is given in the B+F basis B:

$$V_{lB,O_b} = \begin{bmatrix} V_{lx} \\ V_{ly} \\ V_{lz} \end{bmatrix}_B \qquad \Omega_{lB} = \begin{bmatrix} \Omega_{lx} \\ \Omega_{ly} \\ \Omega_{lz} \end{bmatrix}_B \tag{4.10}$$

The velocity vector for the beam center in the basis B is given by the following kinematic formula:

$$V_{lB,O_e} = V_{lB,O_b} + \overrightarrow{O_e O_b} \wedge \Omega_{lB} \tag{4.11}$$

This vector is then expressed in the element basis E:

$$V_{lB,O_e} = P_{EB} V_{lB,O_e} \tag{4.12}$$

4.2.5 Computation of the relative wind velocity at the element center

Now that the wind and local velocities are known, the relative wind velocity reads:

$$V_{rE} = V_{wE} - V_{lE,O_e} \tag{4.13}$$

$$= \begin{bmatrix} V_{rx} \\ V_{ry} \\ V_{rz} \end{bmatrix}_E \tag{4.14}$$

4.2.6 Application of the cross-flow principle

As the cross-flow principle reads, the formulation of aerodynamic loads act as if the spanwise flow velocity component is absent (Zhao et al., 2017). Consequently, the component along the y_e axis of the wind velocity vector is neglected for the drag calculation:

$$V'_{rE} = \begin{bmatrix} V_{rx} \\ 0 \\ V_{rz} \end{bmatrix}_E \tag{4.15}$$

4.2.7 Computation of the wind angle of attack in 2D

To compute the drag force acting on the element, the angle of the upcoming wind on the element must be determined. This angle, called the angle of attack α, is defined as the angle between the wind 2D vector V'$_{rE}$' and the x_e axis of the element. Figure 4.4 describes the α orientation in the (x_e, z_e) plane.

$$\alpha = cos^{-1}\left(\frac{V_{rx}}{\sqrt{{V_{rx}}^2 + {V_{rz}}^2}}\right) \tag{4.16}$$

4.2.8 Computation of drag parameters

From the angle of attack, two key parameters of the drag force acting on the element can be determined: the projected area and the drag coefficient. The frame is composed of beams that have either a rectangular or circular cross section (see Appendix B).

For rounded beams, the drag coefficient is taken constant as 1.17. The projected area is always equal to the diameter D of the beam times the length of the element dy.

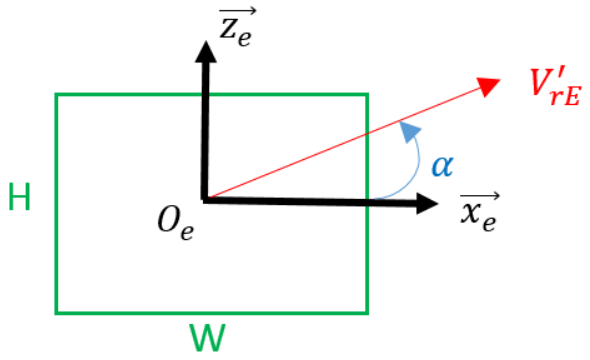

Figure 4.4: Definition of the angle of attack of an element

For rectangular beams, The projected area is given by the Equation 4.17. For the drag coefficient, a table depending on the cross-section dimensions and angle of attack should be established. However, in the implemented code, a generic value of 2.5 is taken for the coefficient at every angle of attack. As the mean wind component is going to be mainly horizontal, the angle of attack should never take high values. This assumption makes the estimation of the load forces conservative, and it is part of the modeling choices that ensure safety factors for the feasibility check.

$$A = dy\big(H|cos(\alpha)| + W|sin(\alpha|\big) \tag{4.17}$$

4.2.9 Computation of aerodynamic loads

The drag force acting on the element can finally be expressed:

$$dF_{D,E} = \frac{1}{2}\rho C_D dy\Big(H|cos(\alpha)| + W|sin(\alpha)|\Big)\big|V'_{rE}\big| \begin{bmatrix} V_{rx} \\ 0 \\ V_{rz} \end{bmatrix}_E \tag{4.18}$$

This force must be expressed in the global coordinate system of basis ϵ:

$$dF_{D,\epsilon} = P_{\epsilon B} P_{BE} dF_{D,E} \tag{4.19}$$

After the establishment of this force for all elements of the structure, it is computed into a three-dimensional force and a three-dimensional moment that is applied at the center of the Blade+Frame body. These force and moment are then communicated to SIMO which incorporates them in the equation of momentum of the body as external forces.

Chapter 5

Results and system responses

In this chapter, the results of the analysis of the system response to different sea states are presented. Thanks to the SIMO modeling, the eigenvalue analysis of the multi-body system is performed, followed by the study of the time-series and spectral responses.

5.1 Eigenvalue analysis

The environmental data used for the establishment of the responses of the system are taken from a 10-year record at the Horn Sea West offshore wind site in the North Sea. This site has a 42m water depth and is located 50km away from the shore. The probability density functions of the main environmental parameters are given in the Figure 5.1. For the wind speed, a factor of 1.51 must be used with the recorded value at the sea level, in order to consider the wind shear effects.

The eigenvalue analysis of the multi-body system is performed with a mean wind speed of 10m/s (which corresponds approximately to the mean value for wind speed 7.56m/s times the shear factor 1.51) and a wind angle of 0°. As it is a static analysis, no wave environment is selected. Wind speed needs to be precised however, since it has force steady mean force component acting on the blade and opposed to the tug line tension force, which need to be taken into account for static equilibrium.

First, a static computation of the model is required. The static results give the equilibrium position for the different bodies of the system. Results are summarized in the Table 5.1. The

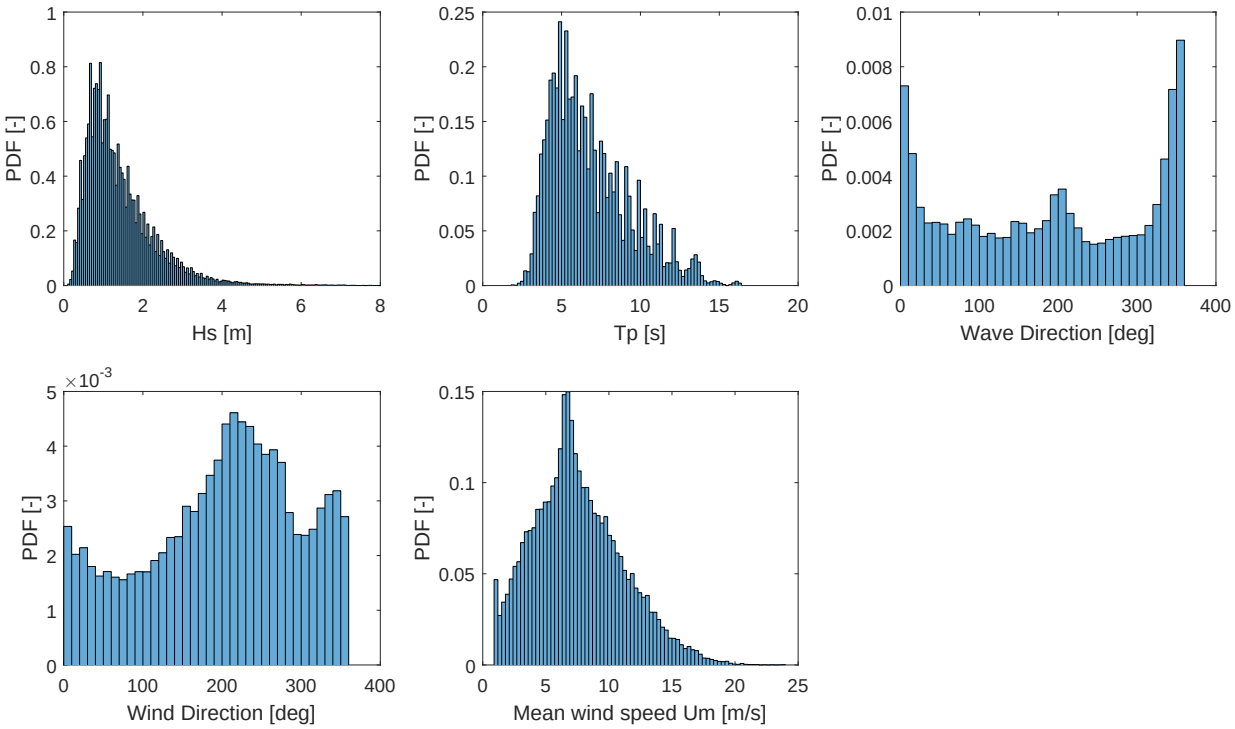

Figure 5.1: Probability density functions of the main environmental parameters at Horn Sea West site from 2001 to 2010. From left to right, up to bottom: significant wave height Hs, peak period Tp, mean wave direction, mean wind direction and mean wind speed (by Yuna Zao).

Table 5.1: Equilibrium position of the bodies

Body	Surge x [m]	Sway y [m]	Heave z [m]	Roll ϕ [°]	Pitch θ [°]	Yaw ψ [°]
Vessel	0.29 e-02	0.79 e-02	-0.014	0.29	-0.05	0.07
Hook	-20.39	-32.72	131.59	0	0	0
Blade+Frame	-21.69	-24.42	110.98	-0.09	3.52	-0.074

Body	Mode	Excursion	0.15	0.33	0.39	0.80	1.21	1.96	2.17	4.88	9.62	10.66	13.58	88.95	98.27	148.77	2.66
OlegS	SURGE	0.30(m)	0.00	-0.00	0.00	-0.00	-0.00	-0.00	-0.00	0.00	-0.03	-0.04	0.00	0.11	-0.47	0.60	0.00
OlegS	SWAY	0.30(m)	-0.00	0.00	0.00	0.00	0.00	-0.00	-0.00	-0.00	-0.00	0.01	0.05	-1.00	0.00	0.06	-0.00
OlegS	HEAVE	0.40(m)	0.00	0.00	-0.00	-0.00	-0.00	0.00	0.00	-0.00	-0.06	0.65	-0.00	0.00	0.00	-0.00	0.00
OlegS	ROLL	0.50(deg)	-0.00	0.00	-0.00	0.00	0.00	-0.00	0.00	-0.00	-0.02	-0.01	0.94	-0.06	0.00	-0.02	-0.00
OlegS	PITCH	1.50(deg)	0.00	-0.00	-0.00	0.00	-0.00	-0.00	-0.00	0.00	0.20	0.16	0.01	0.00	0.00	-0.00	-0.00
OlegS	YAW	0.15(deg)	0.00	-0.00	-0.00	0.00	-0.00	-0.00	-0.00	0.00	-0.00	0.00	-0.01	-0.08	1.00	0.32	0.00
hook	SURGE	4.00(m)	-0.06	0.08	0.01	-0.27	0.20	0.35	0.08	-0.03	0.68	0.53	0.02	0.08	0.07	0.62	-0.03
hook	SWAY	1.50(m)	-0.01	0.00	-1.00	-0.01	0.19	-0.65	0.68	0.01	0.00	0.07	-1.00	-0.51	-0.19	0.02	0.10
hook	HEAVE	0.80(m)	-1.00	0.02	0.03	0.04	0.44	-0.04	-0.03	0.00	0.06	0.84	-0.46	0.02	0.00	0.03	0.02
blade	SURGE	3.00(m)	-0.01	-0.01	-0.00	0.00	0.05	0.57	0.28	-0.20	0.36	0.13	-0.20	0.08	-0.01	0.98	0.04
blade	SWAY	1.00(m)	0.00	-0.00	0.10	-0.00	0.02	-0.29	0.32	-0.02	-0.02	0.09	-0.53	-0.23	-0.11	0.09	-0.30
blade	HEAVE	1.00(m)	0.07	0.01	-0.06	0.02	0.52	0.18	-0.25	-0.01	0.10	0.91	-0.25	0.15	0.05	0.07	-0.19
blade	ROLL	5.00(deg)	-0.06	0.00	-0.46	0.01	-0.38	1.00	-1.00	-0.07	-0.05	0.05	1.00	0.59	0.17	0.13	-1.00
blade	PITCH	2.00(deg)	-0.94	-1.00	-0.07	-1.00	1.00	-0.27	-0.74	0.11	1.00	1.00	0.58	0.06	-0.03	-1.00	-0.31
blade	YAW	5.00(deg)	-0.03	-0.03	0.01	-0.03	0.01	0.44	0.26	1.00	-0.10	0.30	0.71	0.02	0.81	-0.25	-0.17

Figure 5.2: Natural periods [s] and corresponding eigen modes ([m] or [°]) of the system's bodies

positions are expressed in the global reference system of SIMO ϵ (described in Section 4.2.1) whom origin is located at the vessel center.

Because of the tug line pre-tension, the blade and the hook are not directly under the crane tip but shifted towards the direction of the tug lines. This explains why the B+F body has a small pitch angle θ of 3,52 °. The hook rotations are null because it is defined as a single mass body, having only three DoFs: the translation ones. For a reminder of the definition of each motion of the bodies, please see Figures 4.3 and 3.9.

The eigen periods of rigid body motions of the vessel, hook and Blade+Frame are given in the Figure 5.2 along with their corresponding modes. These values are obtained by the resolution of the Equation 2.2 in SIMO. Each natural period can be attributed to one or several specific degrees of freedom. The values enlightened in red in the Figure 5.2 are the predominant modes for each period. Table 5.2 summarized the natural periods associated to the predominant modes of each degree of freedom.

For the vessel, the heave, roll and pitch motions have medium natural periods that are close to the periods of the waves considered, while surge, sway and yaw motions have very large natural periods, way beyond the scope of wave periods. This means that the response motions of the vessel in heave, roll and pitch are the predominant ones, and will therefor be critical when studying the feasibility of the operation.

Table 5.2: Natural periods associated to the predominant modes

Body	DoF	Natural period [s]						
Vessel	Surge	98.27	148.77					
	Sway	88.95						
	Heave	10.66						
	Roll	13.58						
	Pitch	9.62	10.66					
	Yaw	98.27						
Hook	Surge	9.62	148.77					
	Sway	0.39	1.96	2.17	13.58	88.95		
	Heave	0.15	10.66					
Blade+Frame	Surge	1.96	148.77					
	Sway	13.58						
	Heave	10.66						
	Roll	1.96	2.17	2.66	13.58			
	Pitch	0.15	0.33	0.80	1.21	9.62	10.66	148.77
	Yaw	4.88	98.27					

For the B+F body, we can first notice that the sway motions are dominated by the roll motions of the vessel with a natural period of 13.58s. This period corresponds also to the pendulum motions of the lifted body, as it is also related to an important mode for roll motion. The surge motions have two predominant periods, 1.96s which is small because of the impact of tug lines, and 148.77s which corresponds to the vessel natural period in surge as well. The heave motions of the lifted body are governed by the heave motions of the vessel with a natural period in the range of wave periods, 10.66s. The pitch motions are related to multiple natural periods. The impact of the lifting system and the tug line effect can be seen in the smaller natural periods (0.15, 0.33, 0.80 and 1.21s), while the 9.62 and 10.66s periods are due to the natural response in pitch of the vessel. The same conclusion can be drawn for the yaw responses.

5.2 Time-series analysis

For estimating the impact of different environment parameters, five simulations in time-domain of 700s are analyzed. These tests are summarized in Table 5.3. The first two tests have fixed vessel, no waves and a constant wind of 10m/s and 5m/s respectively. Then, the third test has floating vessel, no waves and turbulent wind of 10m/s. The fourth has waves of Hs=2m and

Table 5.3: Description of the tests environmental parameters

Test number	Vessel	Wind	Mean wind speed [m/s]	Waves	Hs [m]	Tp [s]
1	Fixed	Constant	10	None	-	-
2	Fixed	Constant	5	None	-	-
3	Floating	Turbulent	10	None	-	-
4	Floating	Turbulent	10	Yes	2	9
5	Floating	None	10	Yes	2	9

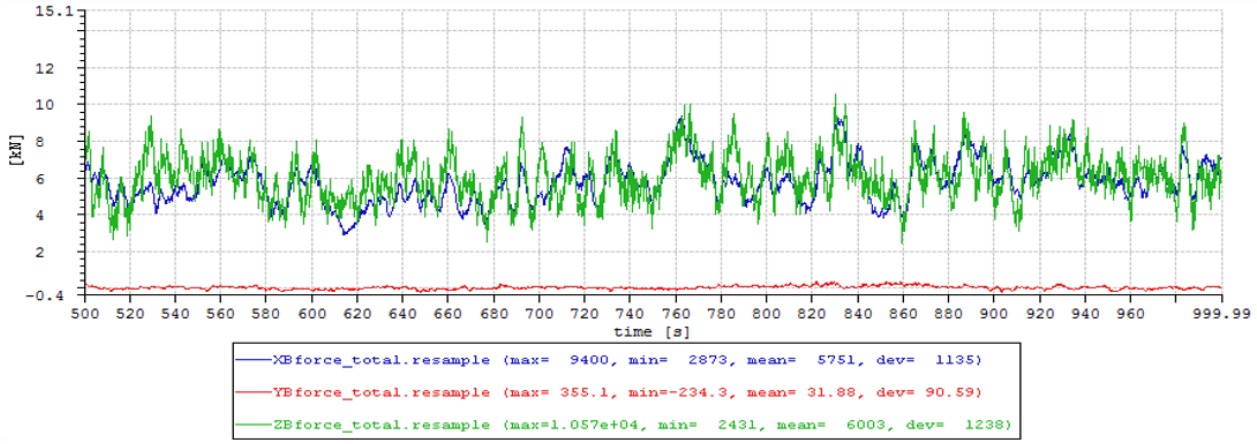

Figure 5.3: Wind force on the Blade+Frame body - Test 4

Tp=9s in addition to the turbulent wind of 10m/s. The last one has waves of Hs=2m and Tp=9s and no wind. In these cases, the impact of wave and wind direction is not estimated. Consequently, mean wave and wind direction are both taken as having 0° angle with the vessel's main axis. Wind and waves are both coming from the stern of the vessel.

The figures from 5.3 to 5.9 show the time-series of the most interesting results of the multi-body analysis. These time-series correspond to the test 4, which is the most complete test since it consider both wind and waves. The time-series for the other tests are given in the Appendix C.

[Figure 5.3 and Figure C.1]. The wind force acting on the B+F body has constant values 6.1 and 6.3 kN for drag and lift respectively for a constant horizontal wind speed of 10m/s (test 1). For 5m/s, these values drop to 1.5 and 1.6 kN, as they are proportional to the square of the wind speed (test 2). For turbulent wind, the mean force values are close to the one for constant wind. However, the turbulence induces high variations in the force components, proving the interest of considering them for the feasibility of the operation. When no wind is applied (test

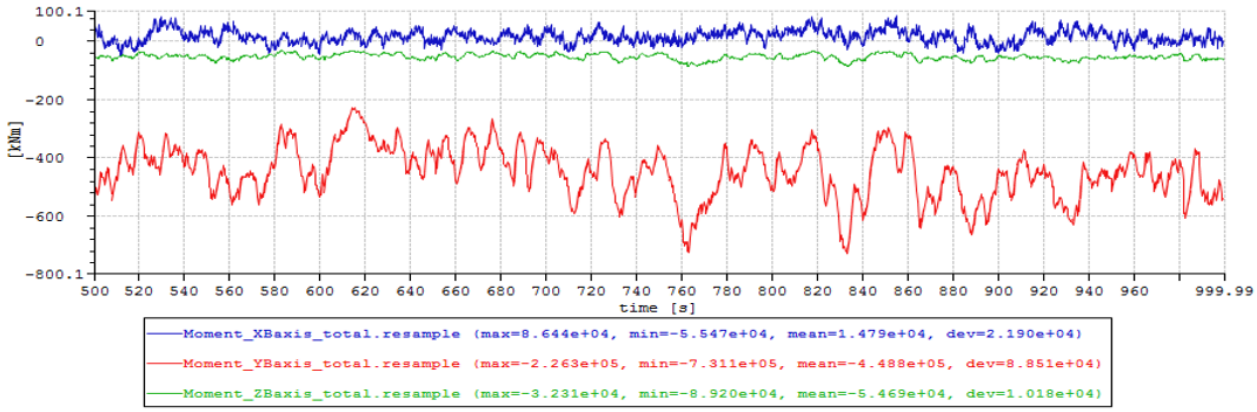

Figure 5.4: Wind moment on the Blade+Frame body at blade center of gravity - Test 4

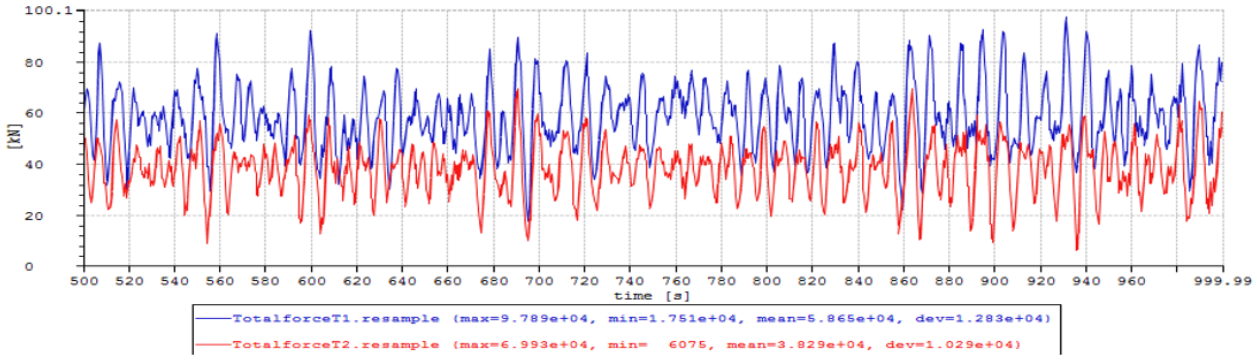

Figure 5.5: Tension force in tug lines - Test 4

5), the wind force is very small because it is only created by the inflow of the B+F wave-induced motions. This is verified in the test 3 and 4, that have the same range of values for wind force components. Finally, the cross-flow principle is correctly applied, and the transverse wind force is almost null in all the cases.

[Figures 5.4 and C.2]. Most of the conclusions drawn for the wind force are also relevant for the wind moment analysis. However, the predominant component is the moment in pitch which is due to the lift force acting on every blade element in the same direction. The absence of transverse wind force on each element explains why the moment in roll is neglectable. The moment in yaw is due to the asymmetry of the B+F body.

[Figures 5.5 and C.3]. It is important to avoid stack in tug line during the operation. For this matter, the tension in the tug lines must not reach the value 0. In the 5 cases tested, including the ones with high waves that are largely beyond the limiting sea state for this operation, tug line

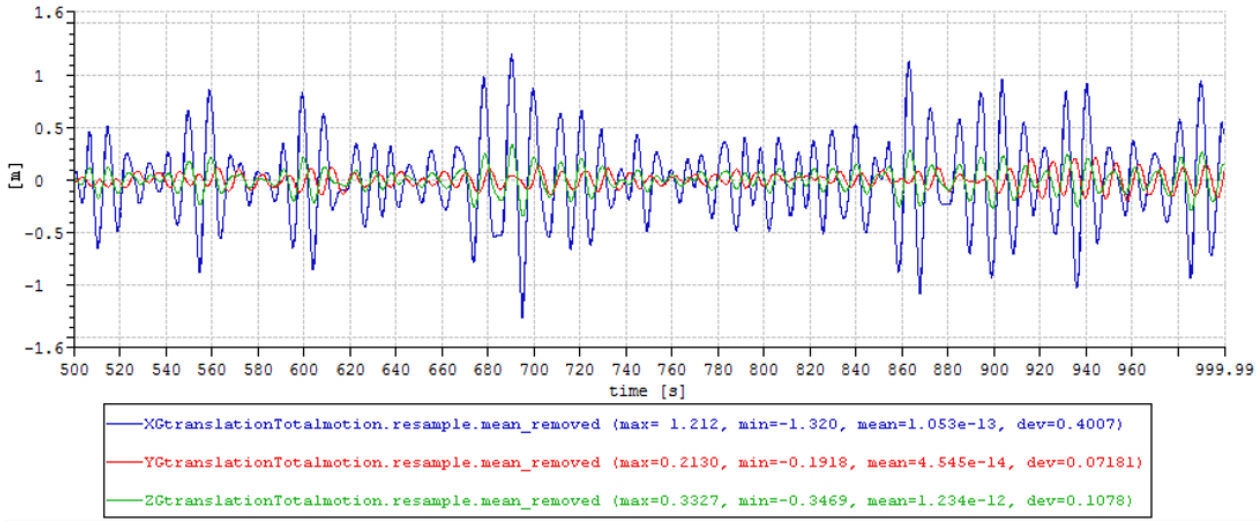

Figure 5.6: Transversal displacement of the blade+Frame body at the blade CoG - Test 4

stack is not happening. This is comforting the relevance of the operation considered. Waves and wind have a high influence on the variations of the tensions, and the worst case is the number 4 with both of them.

[Figures 5.6 and C.4]. For blade CoG translation displacements, the impact of the waves at this sea state are predominant compared to the impact of the turbulent wind. Consequently, it appears that the main limiting parameters for the acceptable sea state may be the one defining the sea states and not the one defining the wind state. These expectations are comforted in the following analyses.

[Figures 5.7 and C.5]. Same conclusions as for the translation displacement. One particularity of the rotational displacement is that the absence of wind in a high sea state is actually worse for the roll motions of the B+F body than having a 10 m/s turbulent wind. The wind is consequently cancelling some wave-induced roll motions, which is particularly interesting for the mating operation.

[Figures 5.8, 5.9, C.6 and C.7]. The predominant vessel displacements in this sea state are in surge, heave and pitch because of the waves direction being parallel to the vessel main axis. There is a high correlation between the vessel displacement curves and the blade displacement ones, proving once more the importance of the wave impact on the feasibility of the operation.

The analysis of the system's time-domain response for different cases showed that the predominant environment effects come from the waves and not the wind. The following of the

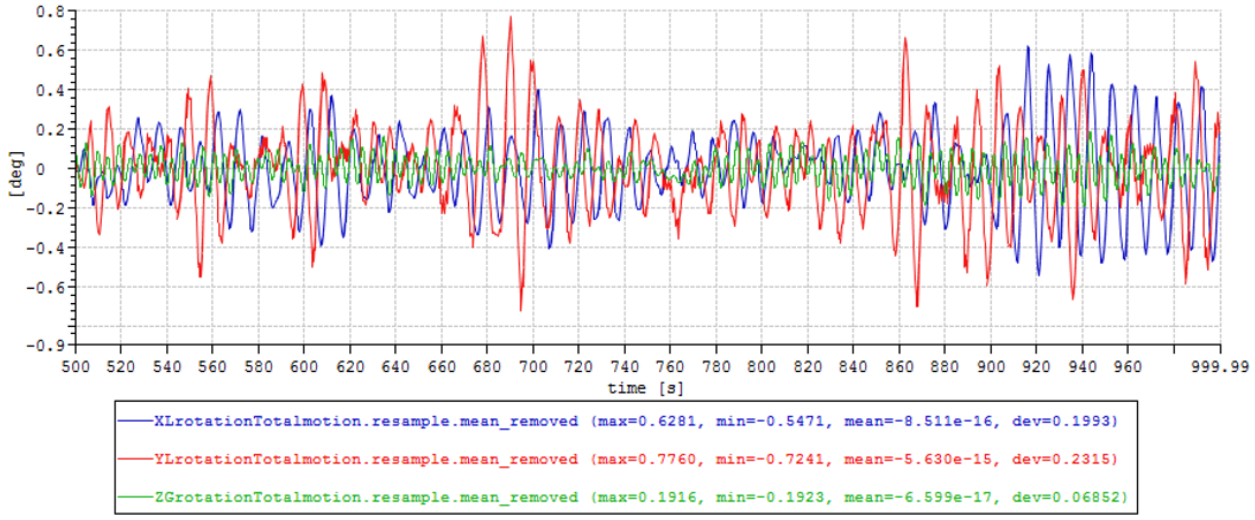

Figure 5.7: Rotational displacement of the blade+Frame body - Test 4

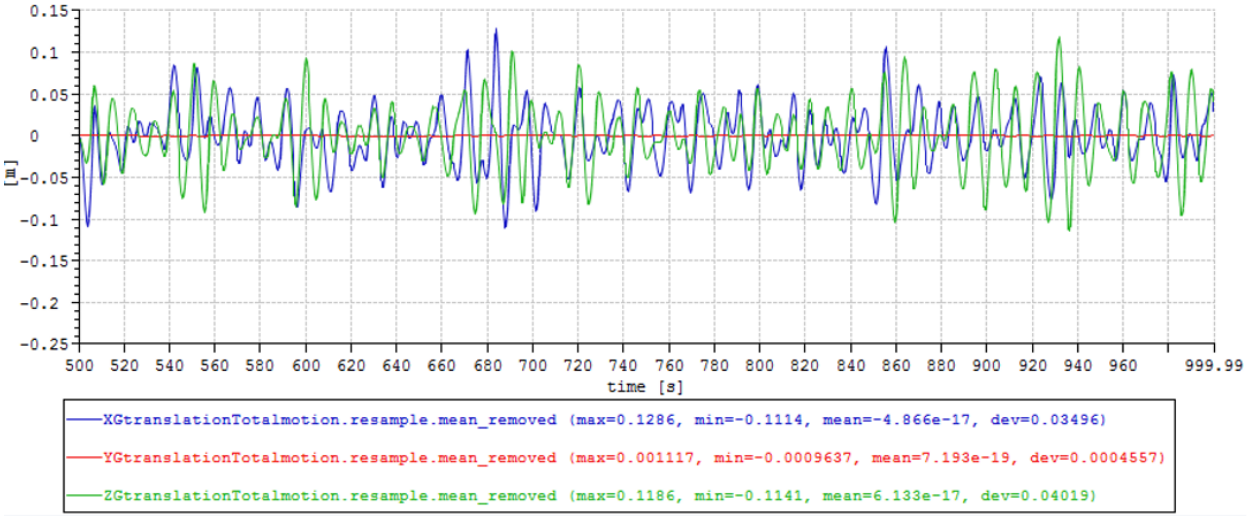

Figure 5.8: Transversal displacement of the vessel at the vessel center - Test 4

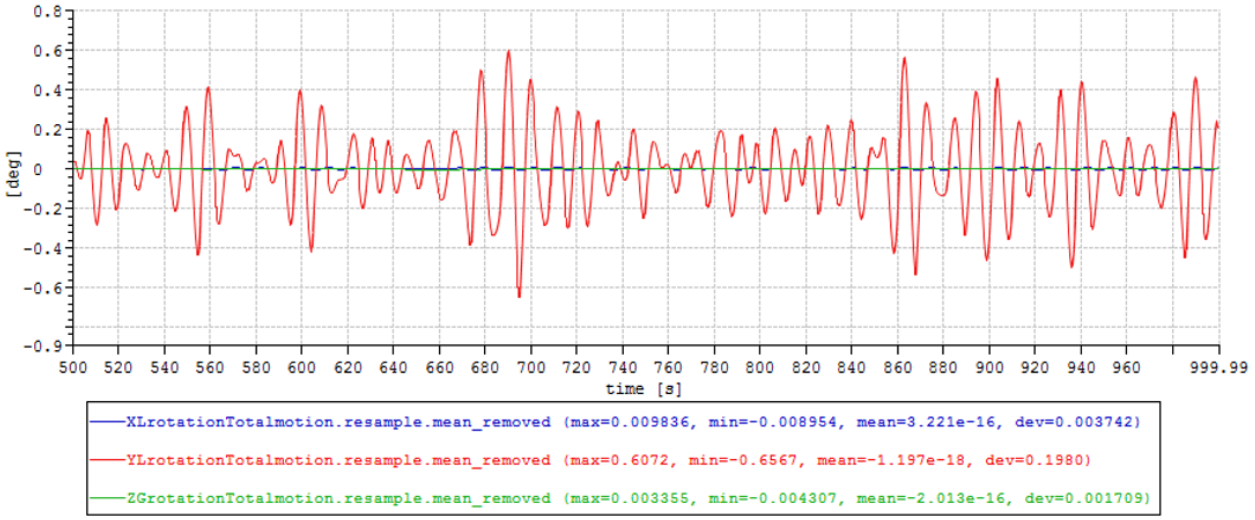

Figure 5.9: Rotational displacement of the vessel - Test 4

study will therefore be focused on the impact of the different wave parameters: the significant wave height, the wave direction and the peak period.

5.3 Spectral responses

The behaviour of the system with different wave parameters is evaluated in this section through a spectral analysis. The comparison is carried out on four cases: one with fixed jack-up vessel, and three with floating vessel and varying sea states. The wind is taken as turbulent with a mean direction of 0°angle and a mean speed of 10 m/s which corresponds approximately to the average wind speed at the installation height (see Section 5.1). To study the impact of the peak period, the second case has a Tp of 8s and the third one of 5,5. The fourth case is aimed to assess the impact of the mean wave angle, and consequently has an angle of 30° while the two others have 0° angle. For the three cases, the significant wave height is taken as 1m.

The most important statistical results for assessing the feasibility of the operation are summarized in the Figure 5.10. It includes the standard deviation of the vessel motions, the mean position of the blade+frame body and the extreme values for the frame tip, where the mating must be performed, the extreme tug line tension and the extreme lifting wire tension. The vessel heave and pitch motions are much higher for the sea states with 8s Tp than for the 5s Tp due to the corresponding natural periods being around 10s. For an non-zero mean wave angle, the

Spectral analysis of governing parameters																		
Case of study (Mean wind speed Uw=10m/s)	Standard deviation for vessel motions						Mean position for blade COG motions						Extreme values for frame tip motions			Extreme values for tug line tension T1 [kN]	Extreme values for lifting wire
	XG [m]	YG [m]	ZG [m]	XL [°]	YL [°]	ZL [°]	XG [m]	YG [m]	ZG [m]	XL [°]	YL [°]	ZL [°]	XA [m]	YA [m]	ZA [m]		
Jack-up vessel	0	0	0	0	0	0	-21,71	-24,40	110,98	-0,089	3,516	-0,082	0,052	0,119	0,131	80,42	1091,552368
Floating vessel with sea state Hs=1m & Tp=8s	0,01322	0,00035	0,01534	0,00202	0,06659	0,00219	-21,68	-24,41	110,98	-0,085	3,516	-0,075	0,498	0,140	0,232	82,88	1098,77771
Floating vessel with sea state Hs=1m & Tp=5,5s	0,01159	0,00035	0,00462	0,00182	0,01758	0,00219	-21,68	-24,41	110,98	-0,086	3,516	-0,075	0,177	0,115	0,122	84,96	1093,833862
Floating vessel with sea state Hs=1m & Tp=8s and theta=30°	0,013612	0,005848	0,014664	0,030259	0,078568	0,016291	-21,6882	-24,4138	110,9777	-0,08291	3,523388	-0,07489	0,529239	0,768906	0,985237	87,8801651	1099,668701

Figure 5.10: Statistical results for the governing parameters

roll and yaw motions are up to 15 times higher than for the case with zero angle. This is critical for the operation since roll motion is having a high impact on the lifted body response. This trend is comforted when analyzing the extreme values at the frame tip. The frame tip is where the hanging points are located, which must be mated with precision on the tower ring hooks. However, only the frame tip motion values for the case 3 with Hs=1m and Tp=5.5s seems to be acceptable. The extreme value for frame tip heave displacement reaches 0.9m for the case 4, which is greatly beyond the acceptable range.

The spectra of the frame tip motions are plotted in the Figures 5.11 5.12 and 5.13. These spectra, in addition to the ones included in Appendix C, give a better understanding of the tip motion causes. When looking at tip motions, the spectra are more complex than the ones for translation motions of blade's CoG, because they combine the responses for translation and rotational motions of the blade's CoG.

In these spectra, the wave frequencies are clearly visible. They are centered around 0,125 Hz and 0.181 Hz for the case of TP=8s and 5.5s respectively. The second order wave effect at the frequency 2f, respectively 0.25 and 0.36s are however not visible probably due to the mooring lines and stiffness response of the vessel. For each motion, the peak corresponding to the natural frequency from the eigenvalue analysis is clearly present.

For the frame surge tip motion, the spectra are showing the peaks of the blade's CoG surge motions close to the wave frequencies but also the peak at 2.2s from the CoG yaw motion. It is first interesting to notice that for some motions of the blade's CoG, the amplitude of responses is much smaller when the vessel is fixed, for example for surge and pitch motions. We can thus conclude than the surge motion of the blade is a direct consequence of the waves.

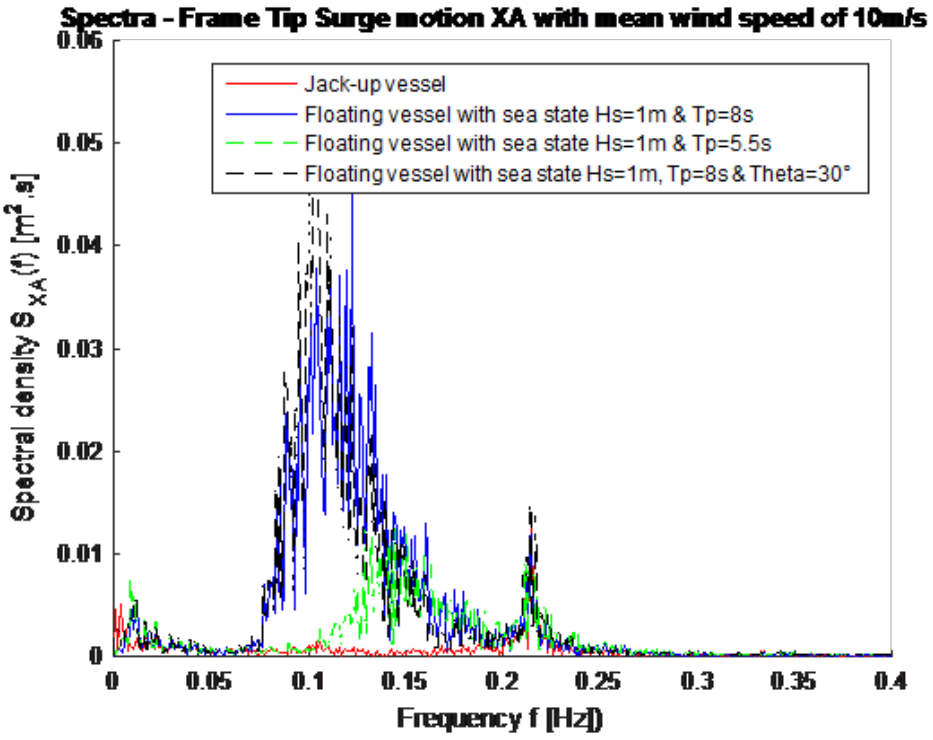

Figure 5.11: Spectra - Frame tip surge motion XA

While the impact of mean wind angle is limited for tip surge motion, it is greatly impacting the tip sway and heave motions.

Figure 5.14 shows the displacement of the frame tip in the (x,z) plane. The trend that has been visible in the previous part of the analysis of the system response is comforted: increasing the peak period and the mean wave angle reduces the accuracy of the mating. Now that the behavior of the frame and its tip is fully understood, the analysis must focus on the assessment of the allowable sea states to perform the operation safely.

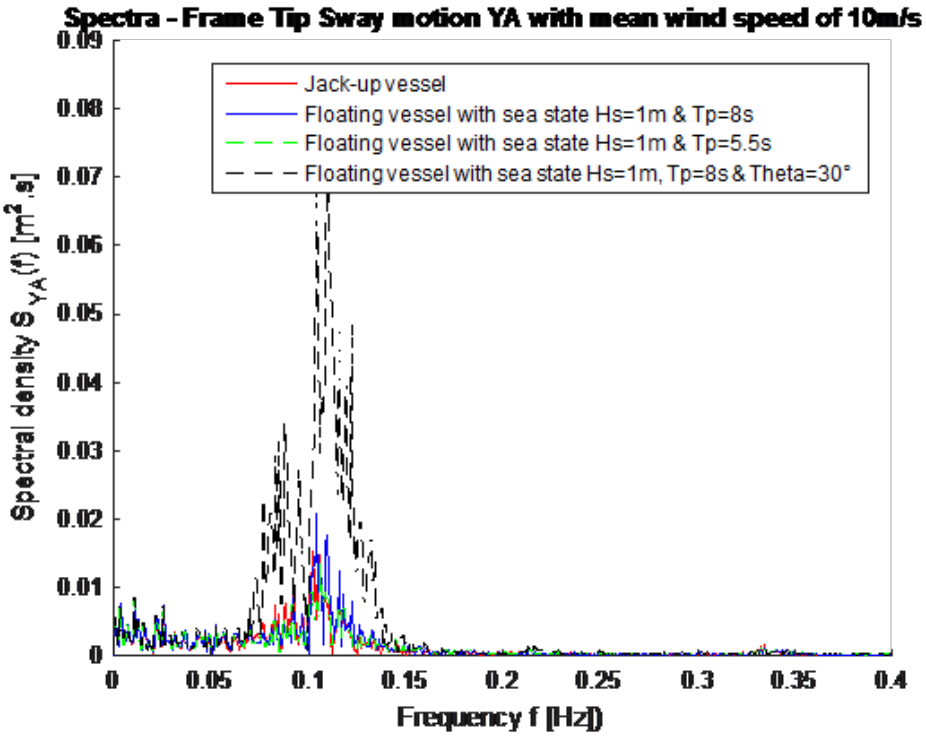

Figure 5.12: Spectra - Frame tip sway motion YA

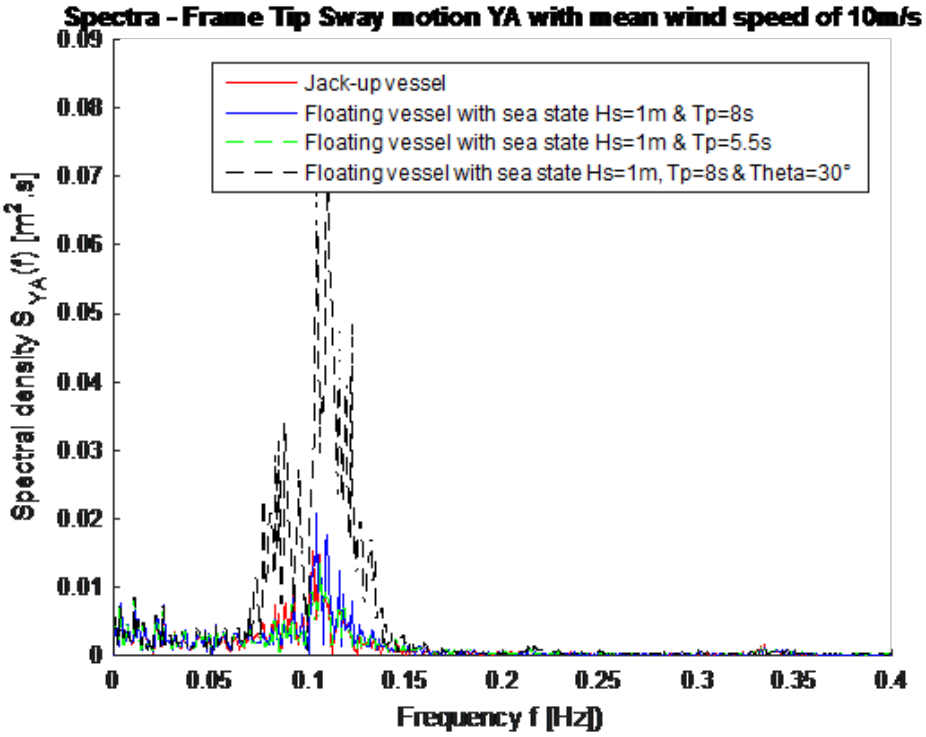

Figure 5.13: Spectra - Frame tip heave motion ZA

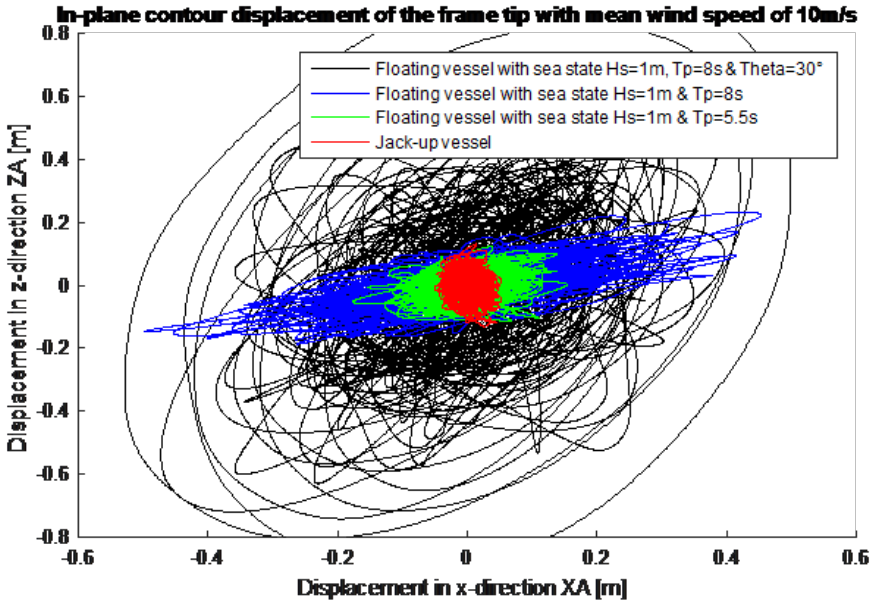

Figure 5.14: In-plane contour displacement of the frame tip

Chapter 6

Estimation of the limiting environmental conditions

In this section, the allowable sea state for performing the operation safely are assessed. A example of a weather window analysis for determining if the operation can be performed during a period of time is given. Finally, the feasibility of the operation is compared to the one of the jack-up installation.

The methodology for assessment of the limiting sea state follows the guidelines of Acero et al. (2016). Figure 6.1 shows the steps that must be followed for an appropriate operational limit assessment.

6.1 Limiting criteria for the mating operation

The main interest of using the tower ring concept (De Groot, 2015) is the facilitation of the mating of the turbine on the tower. Indeed, for a classic blade/rotor mating, the operation consists in fitting the blade bolts in corresponding conic holes of the rotor. Bolts and holes are dispatched in a circle, and they must be mounted all at once. This operation requires a high degree of precision, precision that can be hard to achieve with a floating vessel and its wave-induced motions.

With the tower ring, however, a hang-off system with two hanging points located on the two beams of the frame is sufficient. The mating of the hang-off points is eased using vertical

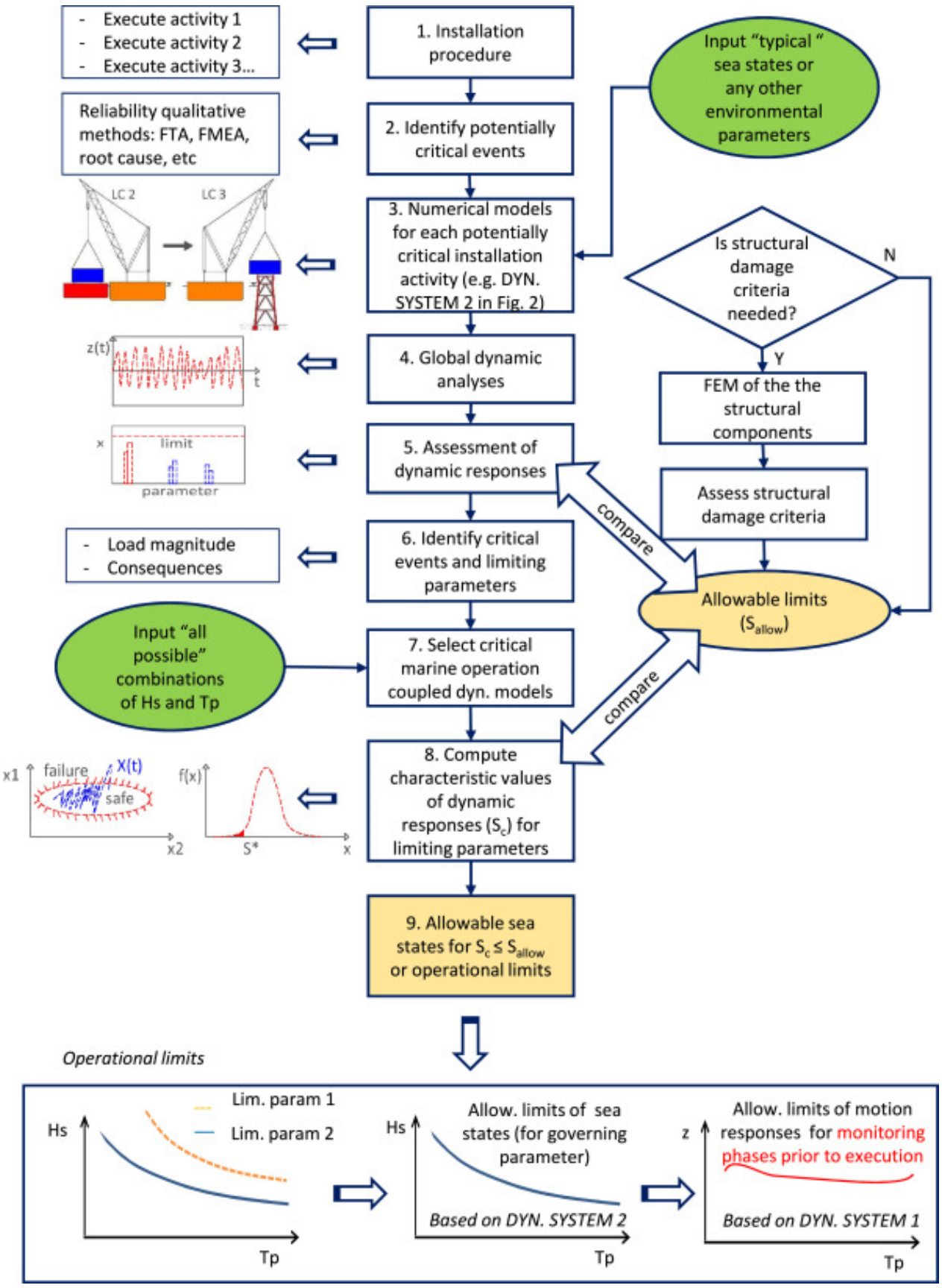

Figure 6.1: General methodology to establish the allowable limits of seastates (Acero et al., 2016)

guides, bumpers and stops. Once the frame is connected to the ring by the hang-off points, only one degree of freedom remains: the rotation around the hanging axis. After lowering the frame around this rotation, bumpers at the rear end of the tool supports the tower and cancel this last degree of freedom. The blade and its frame are thus totally fixed to the tower, and the bolt mating of the blade on the rotor can be performed precisely by shortening the telescoping frame. Once the frame is lowered and standing in the hanging position, the hang-off mechanism is locking it to avoid catastrophic failure when the blade is translated towards the nacelle and then mated. The frame is then released from the installed blade and is installed on the next blade stored on the deck of the vessel.

6.1.1 Description of the mating procedure

First, the frame is lifted in-air, facing the tower ring hanging guides, with no roll, yaw or pitch angle (step 0 on the drawings 6.2). With a translation along the y-axis, the frame bumpers are pushed against the vertical guides of the ring (step1). This contact compensates the translation in y-direction and the rotation around the z-axis. Looking at the top view of the operation, we can see that the hanging points and the hooks are not on the same plane. During the second step, the frame is translated along the x-direction by use of the tug lines, until connection of the bumper stop with the vertical guides (step 2). These stops, together with the tug line at first, and then with the hanging points, are used to compensate the translation in the x-direction. Now the hanging points and the hooks are on the same plane, and it just need to be lowered vertically along the z-axis for the mating (step 3). The hanging connection restrains the degrees of freedom of translation in z direction and rotation around y-axis.

6.1.2 Limiting criteria for mating the frame tips

The critical part of this operation, i.e. the sub-operation that requires the highest precision, is the mating of the hanging points on the hooks. From the geometry of the bodies and the layout of the mating, maximum allowable displacements for the frame tips in x, y and z direction can be extracted. De Groot (2015) does not give a precisely defined geometry for the mating components, and consequently the values for the hanging system dimensions are extrapolated

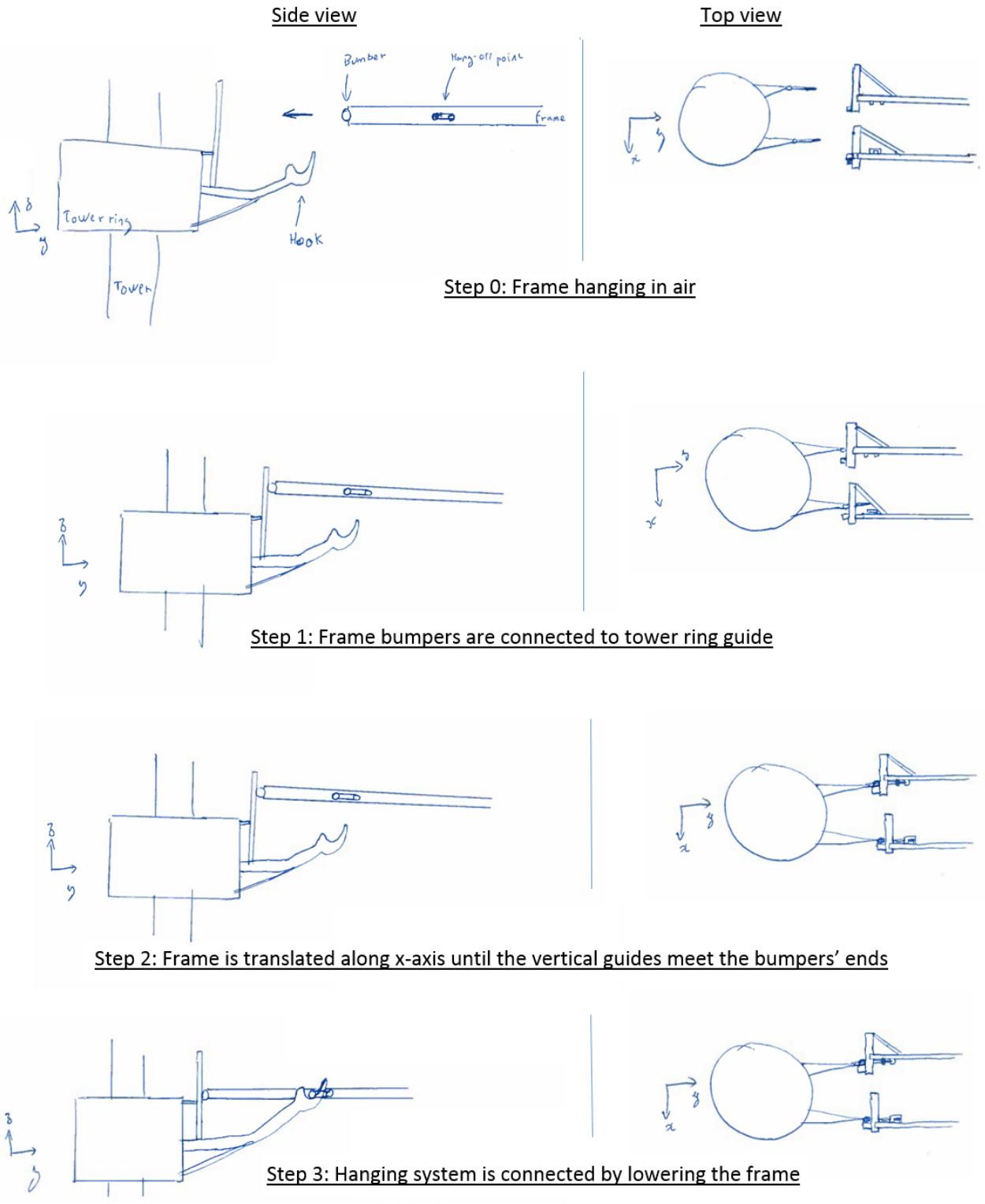

Figure 6.2: Schematic drawings of the mating procedure step-by-step

Table 6.1: Limiting criteria for extreme values of frame tip motions

Motion	Surge XA	Sway YA	Heave ZA
Value [m]	0.2	0.125	0.25

from the technical drawings of his thesis.

We decompose the 3D motion along each axis. Concerning the y direction, it consists of placing the hanging cylinders of diameter 250mm in the 375-mm hook opening (Figure 6.3). This operation is supposedly helped through the pushing of the frame bumpers onto the vertical guides. For a conservative study, the maximum allowable extreme value for displacement is taken as 125mm. It is important to notice that here, the maximum allowable value is given for the extreme value and not the the extreme amplitude of the displacement. This is due to the cancellation of the motion in the direction of the ring due to the contact with the guides. The same procedure is used for the determination of the other maximum allowable values.

In the z direction, while lowering the frame along the vertical guides, a displacement is not as an issue as for the other degrees of freedom. However, when the hanging points are hung on the hooks, the movement induced by the lifting wire before the frame is lowered should be limited to prevent any vertical disconnection. Consequently, the hanging cylinders of 250mm should not go higher than the external end of the hook, i.e. 500mm. The maximum allowable value for displacement is thus taken as 250mm.

In the x-direction, the hook must be clenched in between the hanging points. The space left is 300mm, while the hook thickness is 100mm. As well as for the previous degrees of freedom, the maximum allowable value for the displacement, here defined as 200mm, is conservative. These conservatisms are due to the minimization of the impact of the tug lines pushing the frame's bumper stops against the vertical guides.

To conclude, the maximum allowable values for the three degrees of freedom are summarized in the Table 6.1. These three limiting criteria are used for the determination of the allowable environmental conditions and the weather window analysis.

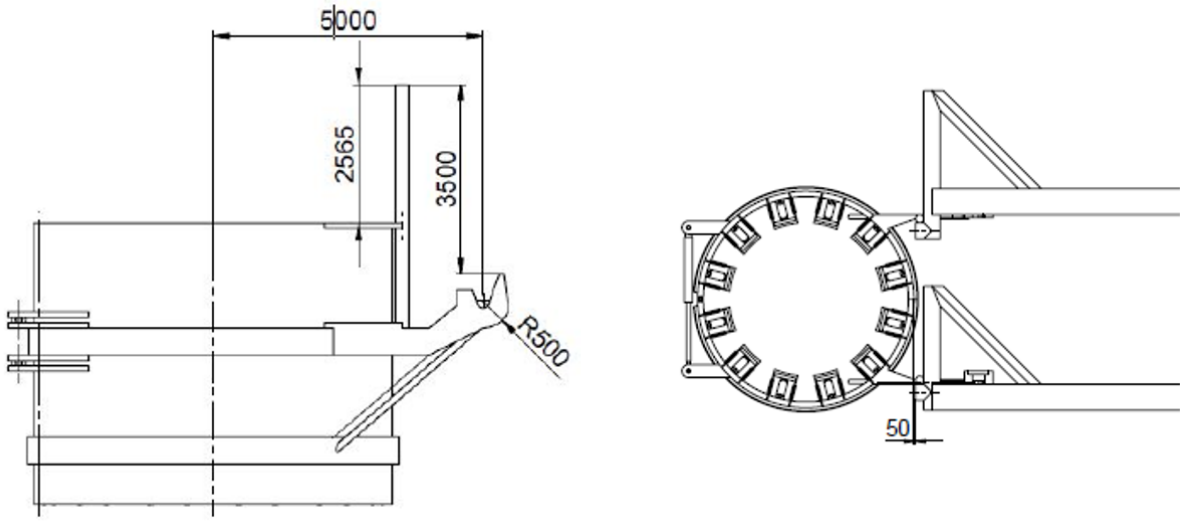

Figure 6.3: Side view (left) and top view (right) of the mating operation (De Groot, 2015)

6.2 Limiting wind and sea states

For estimation of the limiting sea states, multiple simulations must be run with varying parameters. As explained in Section refconfop, three configurations for the angle between mean wave and wind directions are considered: 0_0°, -15_15° and-30_30°. For checking the acceptability of each sea conditions, the average extreme value of five 10mn-simulations is confronted to the limiting criteria defined in the previous section. If one of the three average extreme values for frame tip displacement exceeds the corresponding limiting criteria, the sea state is not accepted. Both surge, sway and heave motions of the tips must be within the acceptable range.

As explained above, the impact of the mean turbulent wind speed value is not the most critical for the operation feasibility. The feasibility assessment is consequently focused only on the limiting sea states. These sea states are described by 3 main parameters: Hs, Tp and the angle with the mean wind direction. The use of three cases of study allows the determination of the impact of the angle between wind and wave directions. The two other parameters are varying for each set of 5 simulations. These five simulations that are used to determine the average extreme displacement values over a 10 mn period have similar environmental parameters but different seeds for waves and wind turbulence.

From the analysis of the environmental data given at the offshore site (see Section 5.1), the

range for Hs and Tp are selected. The sea states used for checking the feasibility have a Tp from 4 to 12s and an Hs from 0.05 to 5m. The mean wind speed is taken as 10m/s since it is approximately the average wind speed at installation height. In figure 6.4, the orange data represent the sea states that induce average extreme value for displacement that are not acceptable. The blue data represent the sea states for which the operation can be conducted safely. The grey data correspond to the intersection of the orange and blue data, and therefor represent the limiting sea states. A power trend is drawn for each case in order to get a better picture of the limits for allowable sea states. Some sea states plotted on these curves are deliberately unrealistic (such as Tp=4s and Hs=8m), but are still present to have a better comprehension of the sea state limit curve. The interesting part of the curves is the one in the range of Tp from 5 to 10s and of Hs from 2 to 0.1m.

The limiting sea states and their corresponding power trend curves are plotted on the same graph in Figure 6.5.

The impact of the wave angle is critical for the feasibility of the operation. For 0° angle, the allowable sea states are reaching values of Tp and Hs that are similar to other highly weather-sensitive operations. However, as soon as a mean wave angle is introduced, the pool of allowable sea states for the operation is shortened drastically. In these cases, the operation needs a very calm sea for being operated. It is interesting to notice that having an angle of 15° or 30° is not having a strong impact on the limiting sea states. The main difference is between sea states with no wave angle, and sea states with a non-zero wave angle.

6.3 Weather-window estimation

When a marine operation is planned, a weather window estimation is performed. Knowing the weather forecast for the next hours, days or weeks, the engineer can estimates if the operation can be performed safely and when. A example of the use of this paper's results for a weather window analysis is given in this section.

First, the operational time of the blade mating is estimated to be 4.2 hrs (De Groot, 2015). A extra time of half the operational time is usually added in marine operation design to consider uncertainties in the operation. The total time is therefore 6.3 hrs. With the available weather

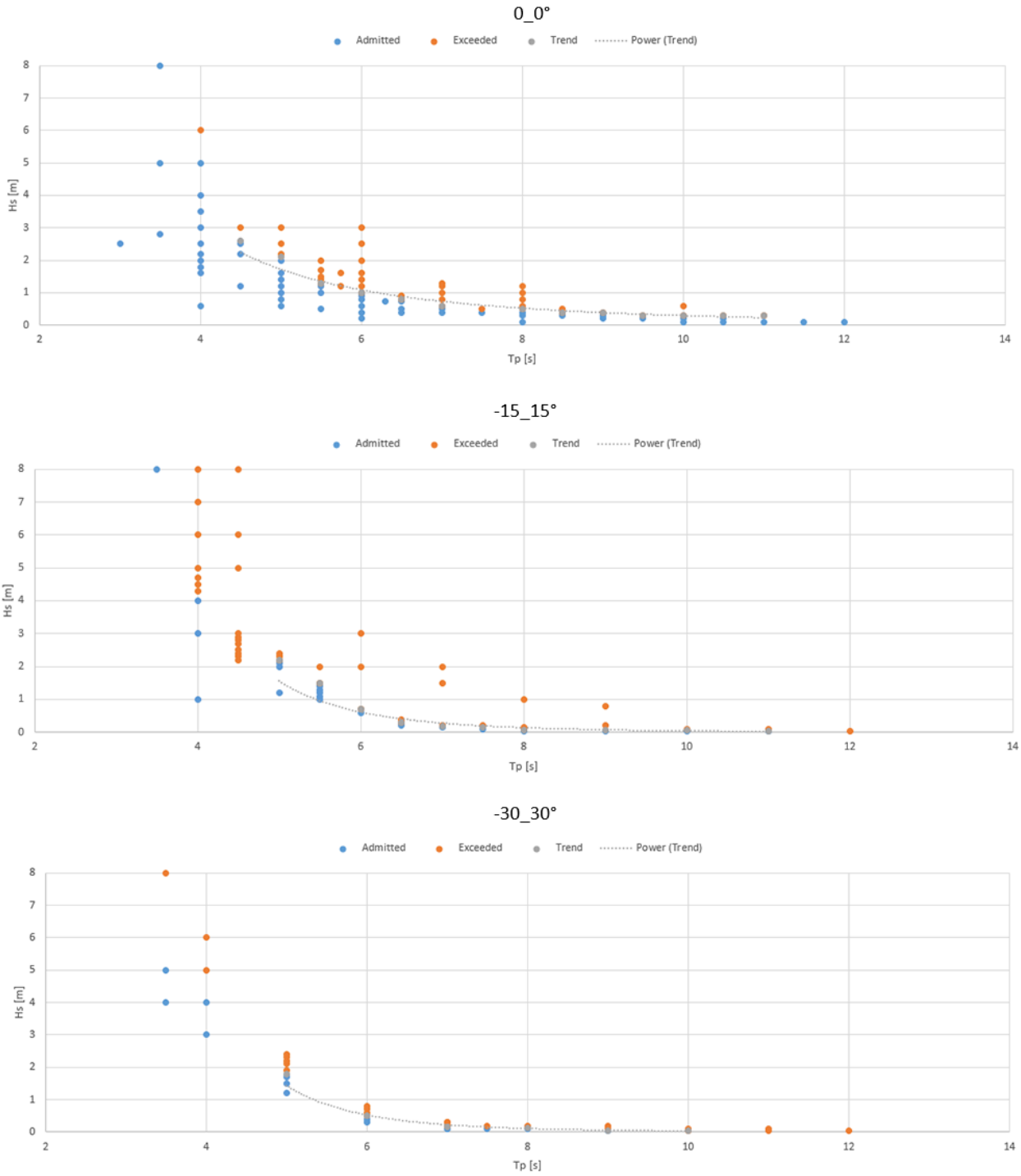

Figure 6.4: Assessment of the allowable sea states for the three cases. From top to bottom, case 0_0, case -15_15 and case -30_30

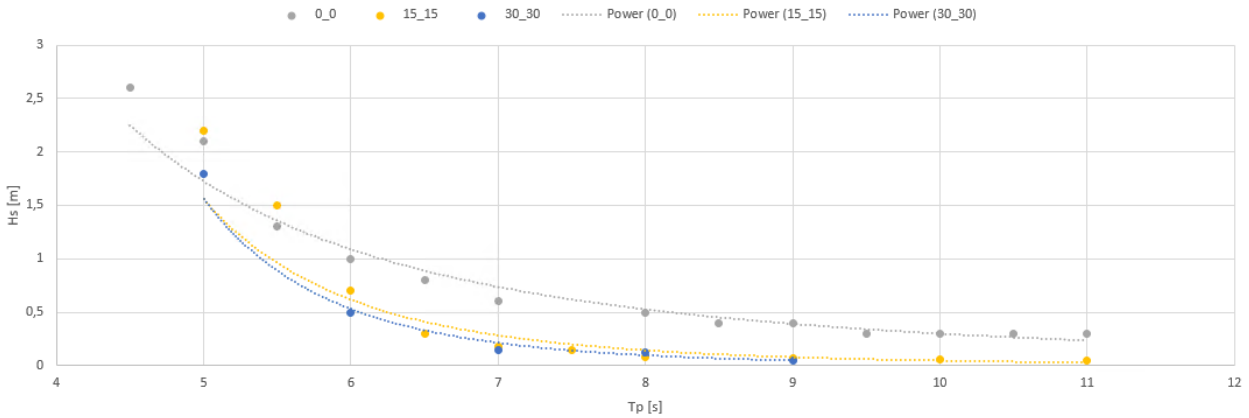

Figure 6.5: Limiting sea states and their corresponding power trends for the three cases

forecast, the engineer looks for a window of 6.2 hrs of calm sea state. Calm sea states are defined as sea states whose parameters are below the limiting sea state curves, with the considering of an extra factor for uncertainties in the precision of the forecast. The weather forecast is then confronted to the limiting sea states established in this paper, and if a time-window of calm sea state is sufficiently large for the total operational time, then the operation is allowed to be conducted. However, since the limiting sea states estimated in this paper are based on 10 mn simulations, the weather forecast must be given by 10 mn periods. It is often given hour by hour but the weather window analysis can still be conducted by considering that the six 10 mn periods of each hour have the same environmental parameters than the ones of the corresponding hour.

6.4 Comparison with jack-up vessel

Jacking operations are highly weather sensitive operations since the legs must be deployed to the sea bed. However, some jacking operations can be performed with a sea state having a Hs up to 1m (2m for some state-of-the-art vessels). These operations accepts multiple Tp, from 4 to 12s. In comparison with the results for the floating vessel, jack-up vessel are less sensitive to the sea states and can consequently operate the blade mating during more time within a year than the floating installation vessel. Indeed, in the best case for the floating vessel (0° angle for the wave direction), at Tp of 8 to 10s, the operation can be performed with sea states having an

Hs less than 0.5m, which is quite low. In the worst cases (small angles for the wave direction), the operation can be performed in very limited sea conditions.

However, the time for installing a full turbine is almost reduced by half with the introduction of floating vessel. One of the perspective of this study can be the estimation of the pro and cons of reducing the operation duration by having more limited allowable sea states.

Chapter 7

Summary

This Chapter concludes the analyses done in this report and draw the conclusions and perspectives regarding the results.

7.1 Conclusions and discussions

By the modeling of an innovative method for installing OWT's blades with a floating installation vessel, this paper is aimed to challenge the current trends of the industry to use jack-up vessels for top-turbine installation. This innovative method is based on the use of a tower ring concept that is easing the mating of the blade on the rotor De Groot (2015). In this analysis, a external code for integrating the aerodynamic loads from turbulent wind acting on the lifted blade and frame is added to the SIMO software. The analyses of the behavior of the lifted Blade+Frame body show that the impact of the turbulent wind on the lifted blade is not as critical as the impact of the vessel motions due to the waves. Due to the natural periods of some motions of the lifted object being in the range of the common wave periods, the displacements of the tip of the frame are highly dependent on the sea state. Following the method of Acero et al. (2016), the operation feasibility is assessed by establishing the limiting sea states. These wave-induced motions are even more critical when the waves are coming from the side of the moored installing vessel.

The comparison with the jack-up installation shows that jack-up operations accept limiting sea states of wider significant wave heights and peak periods than the floating vessel installa-

tion. One additional problem of the floating vessel is the mean wave direction, which can limit drastically the allowable sea states when the vessel is not facing the waves. However, the operational time with floating vessels is almost divided by half for a total wind turbine installation compared with the jack-up vessels. The relevance of floating vessels for OWT installation must therefor continue to be investigated.

The analysis performed in this thesis are based on several assumptions due to the modeling and to some uncertainties concerning the operation realization. Therefore, the choice has been done to conduct simulations leading to results with a certain degree of conservatism. One of the main limitation of the work is the neglecting of reduction of the lifted body motions while connected to the guiding system before mating. The integration of the effect of this guiding system in the simulations could lead to results much more satisfying for the limiting sea states.

7.2 Recommendations for future work

The simulations could be more complete and having a smaller degree of conservatism if the impact of the guiding system was considered. An accurate model of the frame and the tower ring system must be implemented, with the analysis of the locking operation step by step.
This thesis focuses only on the mating sub operation for the blade operation. However, it could be interesting to analyze other sub-operations within the blade installation, such as the lifting off the vessel, the lowering of the frame when connected to the tower or the mating of the blade bolts on the rotor with the use of the telescopic beams.
In a future work, the results of this thesis for the limiting sea states can be used to estimate the average time of calm and storms for the operation realization within a year. Then, the analysis can be pursued towards the estimation of statistic results for the probability of blade installation feasibility.

Appendix A

Acronyms

B+F Blade + Frame

CoG Center of Gravity

DoF Degree of Freedom

DP Dynamic Positioning

EU European Union

JONSWAP Joint North Sea Wave Project

OSV Offshore Supply Vessel

OWT Offshore Wind Turbine

SI International System of units

SPAR Single Point Anchor Reservoir

SIMO SImulation for Marine Operation

TLP Tension Leg Platform

WTIV Wind Turbine Installation Vessel

Appendix B

Additional operation description

In this Appendix, more detailed information is given about the parameters used to perform the numerical modeling. It includes hydrostatic data of the vessel, characteristics of the DTU 10MW turbine, frame geometry and dimensions and frame discretization.

B.1 Hydrostatic characteristics of the vessel

The characteristics of the vessel used for the modeling come from the work of Lin Li during her PhD writing at the Department of Marine Technology at NTNU. Table B.1 and Table B.2 represent the linear damping matrix and the hydrostatic stiffness matrix of the vessel respectively. All units are given in the International System of units (SI). The hydrostatic stifnesses are calculated as equivalent stiffnesses including the effect of the mooring lines.

Table B.1: Linear damping of the vessel motion (SI units)

	Surge	Sway	Heave	Roll	Pitch	Yaw
Surge	9.14 e+05	0	0	0	0	0
Sway	0	2.41 e+06	0	0	0	0
Heave	0	0	0	0	0	0
Roll	0	0	0	7.3528e+08	0	0
Pitch	0	0	0	0	0	0
Yaw	0	0	0	0	0	4.05e+09

Table B.2: Hydrostatic stiffness matrix of the vessel (SI units)

	Surge	Sway	Heave	Roll	Pitch	Yaw
Surge	2.585 e+05	0	0	0	0	0
Sway	0	3.411 e+05	0	0	0	0
Heave	0	0	7.0257 e+07	0	7.029 e+08	0
Roll	0	0	0	6.858 e+09	0	-1.763 e+08
Pitch	0	0	7.029 e+08	0	1.453 e+11	0
Yaw	0	0	0	-1.763 e+08	0	7.642 e+08

Rated power	10 MW
Number of blades	3
Rotor Diameter	178.3 m
Hub Diameter	5.6 m
Hub Height	119.0 m
Drivetrain	Medium Speed, Multiple-Stage Gearbox
Minimum Rotor Speed	6.0 rpm
Maximum Rotor Speed	9.6 rpm
Maximum Generator Speed	480.0 rpm
Gearbox Ratio	50
Maximum Tip Speed	90.0 m/s
Hub Overhang	7.1 m
Shaft Tilt Angle	5.0 deg.
Rotor Precone Angle	-2.5 deg.
Blade Prebend	3.332 m
Rotor Mass	227,962 kg
Nacelle Mass	446,036 kg
Tower Mass	628,442 kg

Figure B.1: Key parameters of the DTU 10 MW Reference Wind Turbine - Adapted from Bak et al. (2013)

B.2 Characteristics of the DTU 10MW turbine

The OWT used for the modeling is the DTU 10MW RWT which is free to use and aimed for investigation of wind turbine researches (Bak et al., 2013). The main characteristics of the turbine are given in the Figure B.1. The blade is 87.2m long and its center of gravity is located at 26.33m from the blade root. The blade is not pre-bend and more information about the variation of the cross-sections along the length can be found in the report of Bak et al. (2013).

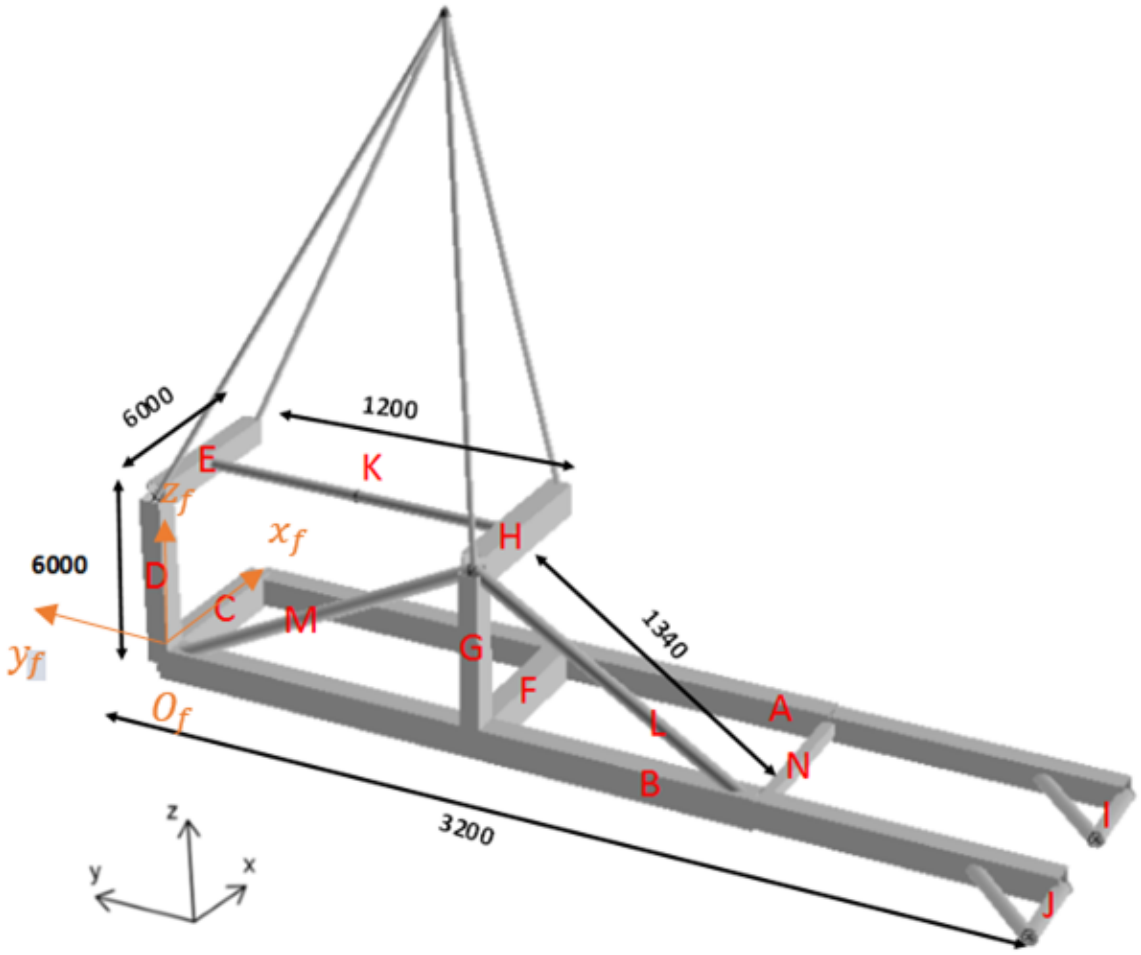

Figure B.2: Frame structure description - adapted from De Groot (2015)

B.3 Frame geometry definition

The structure of the frame is composed 12 main beams as it is depicted on Figure B.2. The beam I and J are the bumpers used for the guiding system of the locking mechanism. Their dimensions are small regarding the other beams, and their impact on the aerodynamic calculation is therefor considered as neglectable. The cross-sections of the other beams are rectangular or circular. Their main dimensions are extracted from the thesis of De Groot (2015) and summarized in the Table B.3 For the aerodynamic calculations, the frame beams are discretized into small elements. This discretization is done along the length of the beams, with constant element length of 2m for beams A ,B, C, D, E, F, G, H, N and 1.92m for beams K, L.

Table B.3: Dimensions of the frame beams -Adapted from De Groot (2015)

Beam name	Cross-section	Length [m]	Height/Diameter [m]	Width [m]
A	Rectangular	32	1.1	0.9
B	Rectangular	32	1	0.9
C	Rectangular	6	1.2	0.8
D	Rectangular	6	0.8	0.9
E	Rectangular	6	0.9	0.7
F	Rectangular	6	1.2	0.8
G	Rectangular	6	0.7	0.9
H	Rectangular	6	1.1	0.85
K	Circular	13.4	0.5	-
L	Circular	13.4	0.5	-
M	Circular	12	0.4	-
N	Rectangular	6	0.7	0.7

Appendix C

Additional results for the response of the system

In the Chapter 5, some time series of the system response and motion spectrum are plotted. In this Appendix, more responses are plotted to give a better picture of the behavior of the system under various sea states.

C.1 Additional time-series results

The time-series results for the 5 cases are plotted in the Figures C.1 to C.7. This curves are commented in Section 5.2.

C.2 Additional Spectra

The Spectra for Blade CoG motions are enclosed in this section (Figure C.8).

Figure C.1: Wind force acting on the B+F body for tests 1 to 5. X-component in blue, Y-component in red, Z-component in green

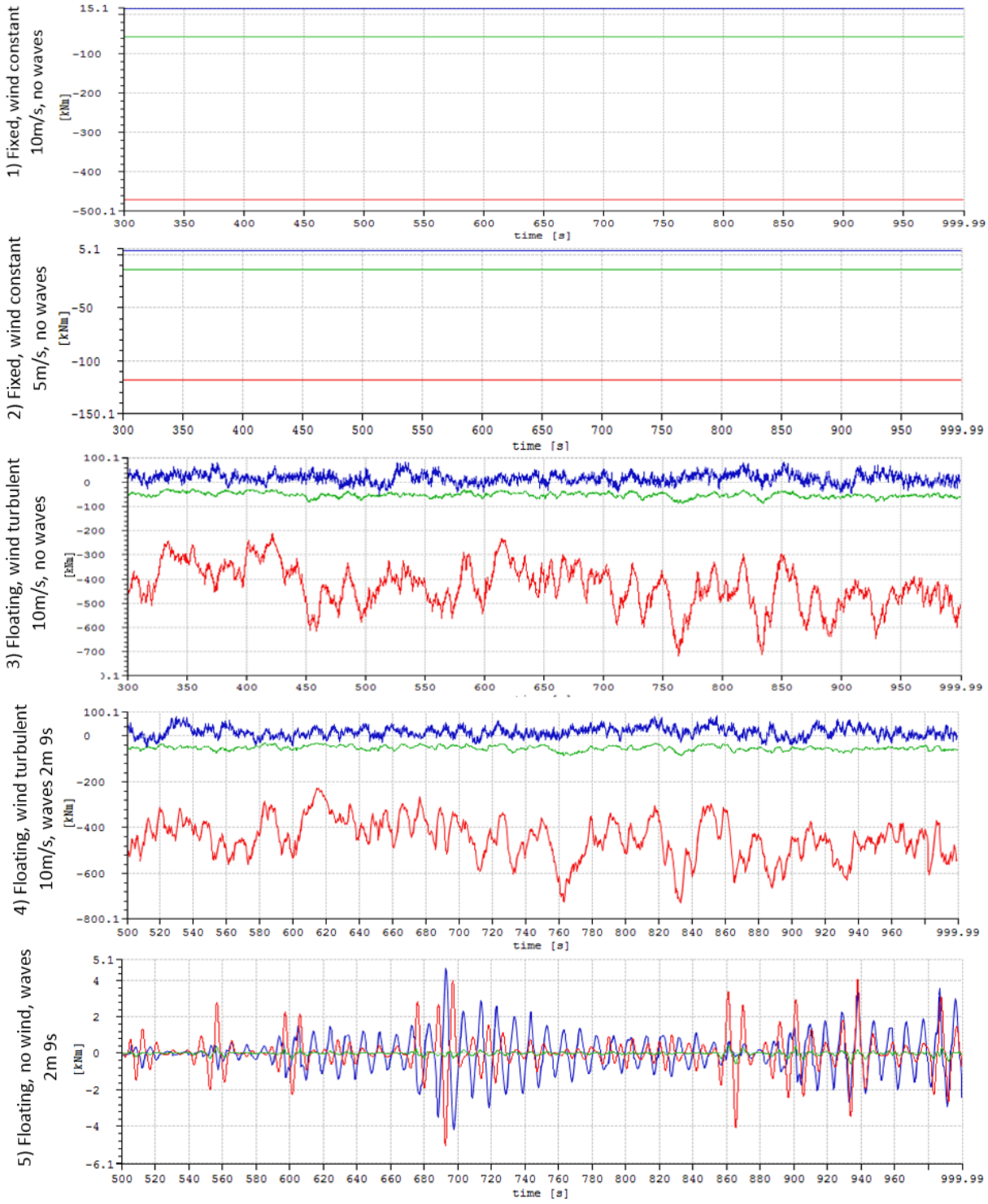

Figure C.2: Wind moment acting on the B+F body at blade CoG for tests 1 to 5. X-component in blue, Y-component in red, Z-component in green

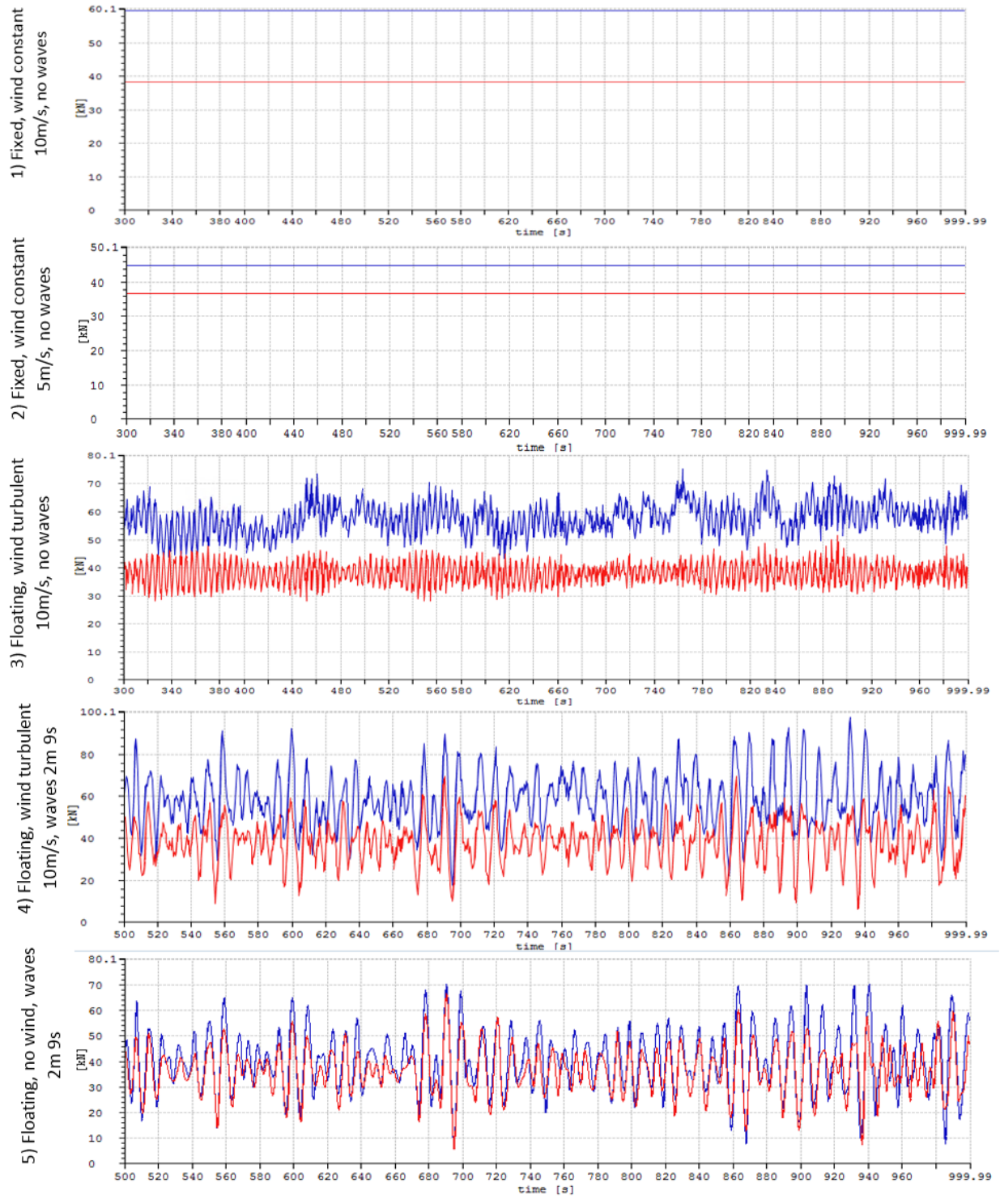

Figure C.3: Tension force in tug lines for tests 1 to 5. Tug line 1 in blue, Tug line 2 in red

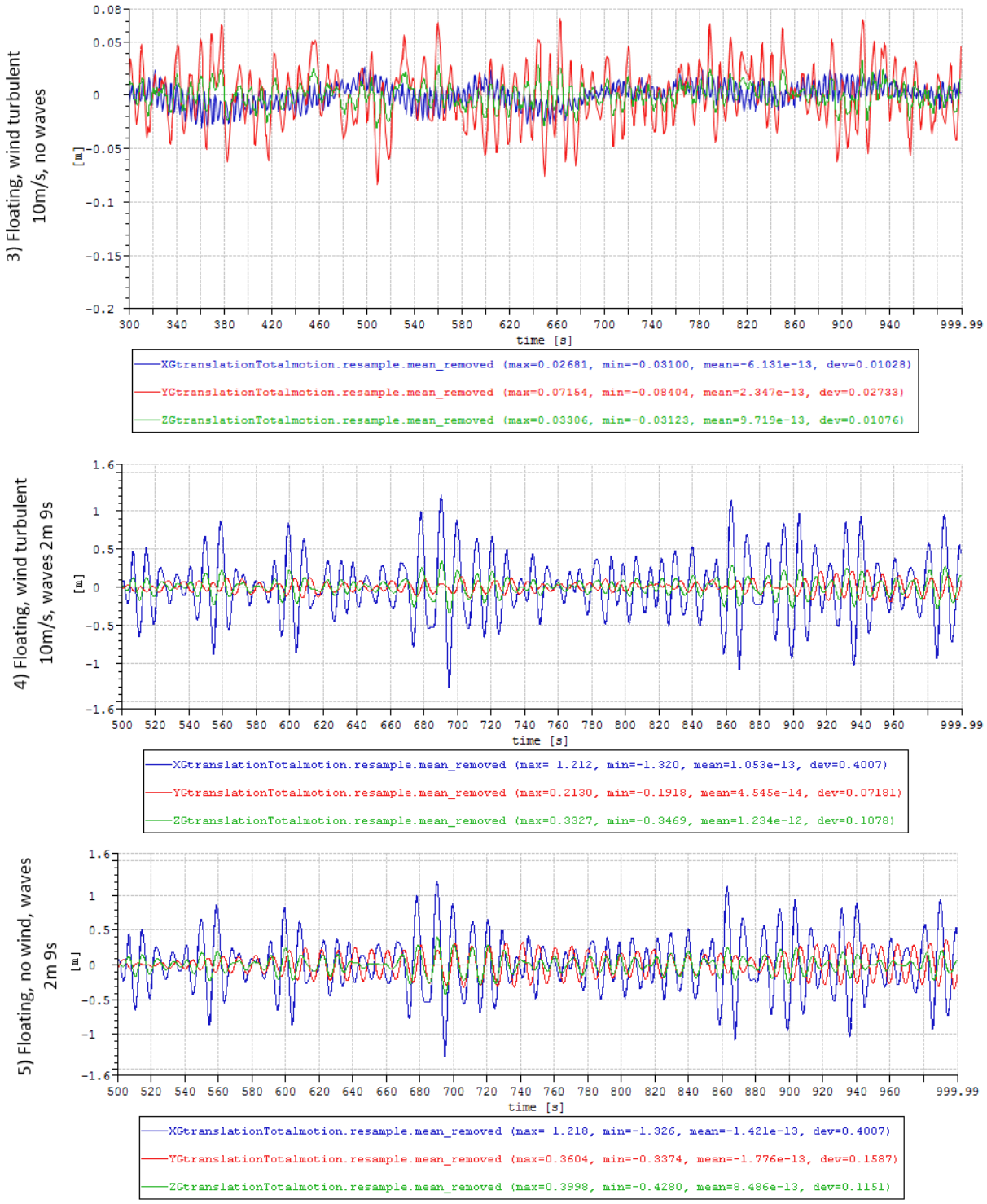

Figure C.4: Translation displacement of the blade+Frame body at the blade CoG for tests 3 to 5. X-component in blue, Y-component in red, Z-component in green

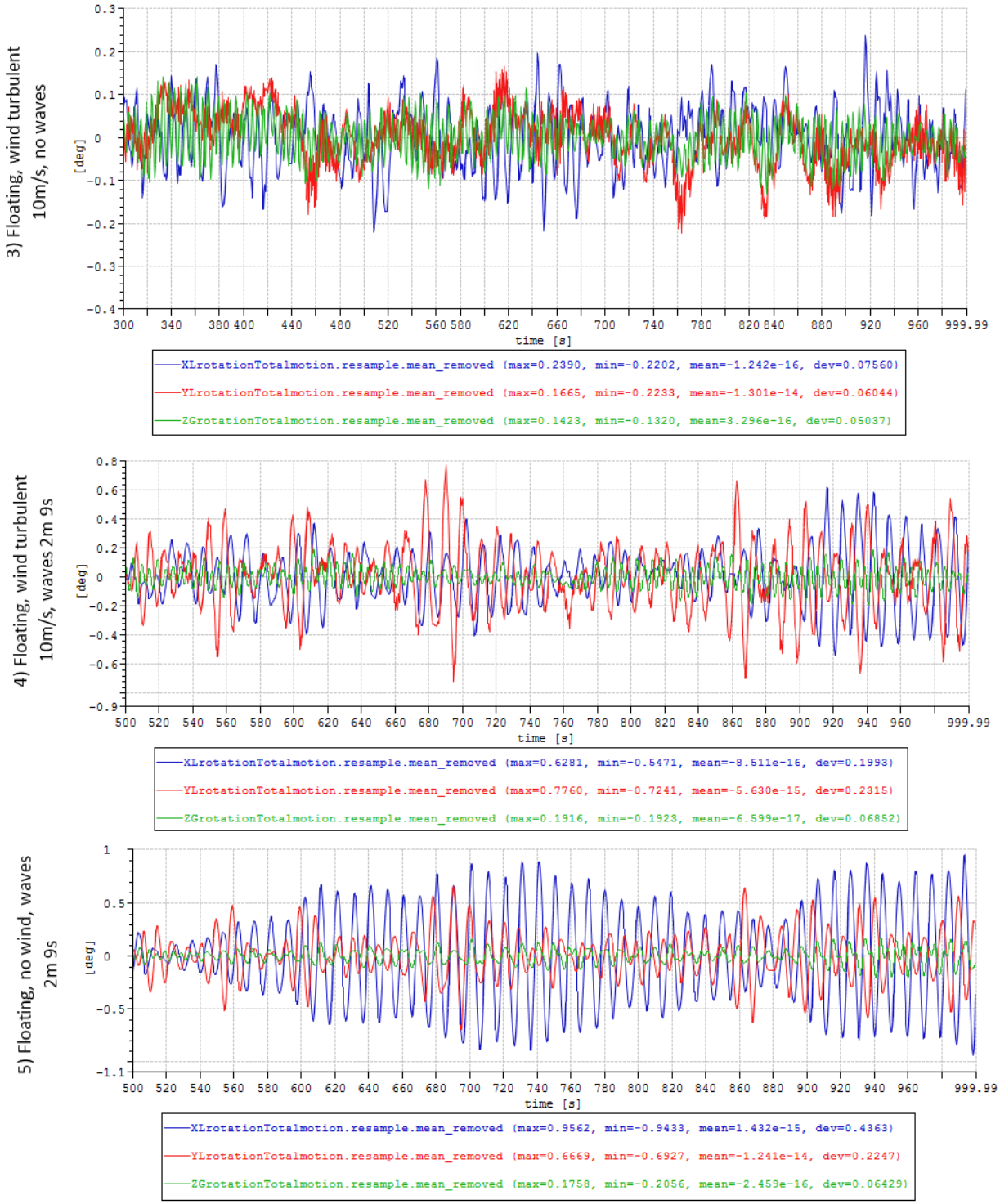

Figure C.5: Rotational displacement of the blade+Frame body for tests 3 to 5. X-component in blue, Y-component in red, Z-component in green

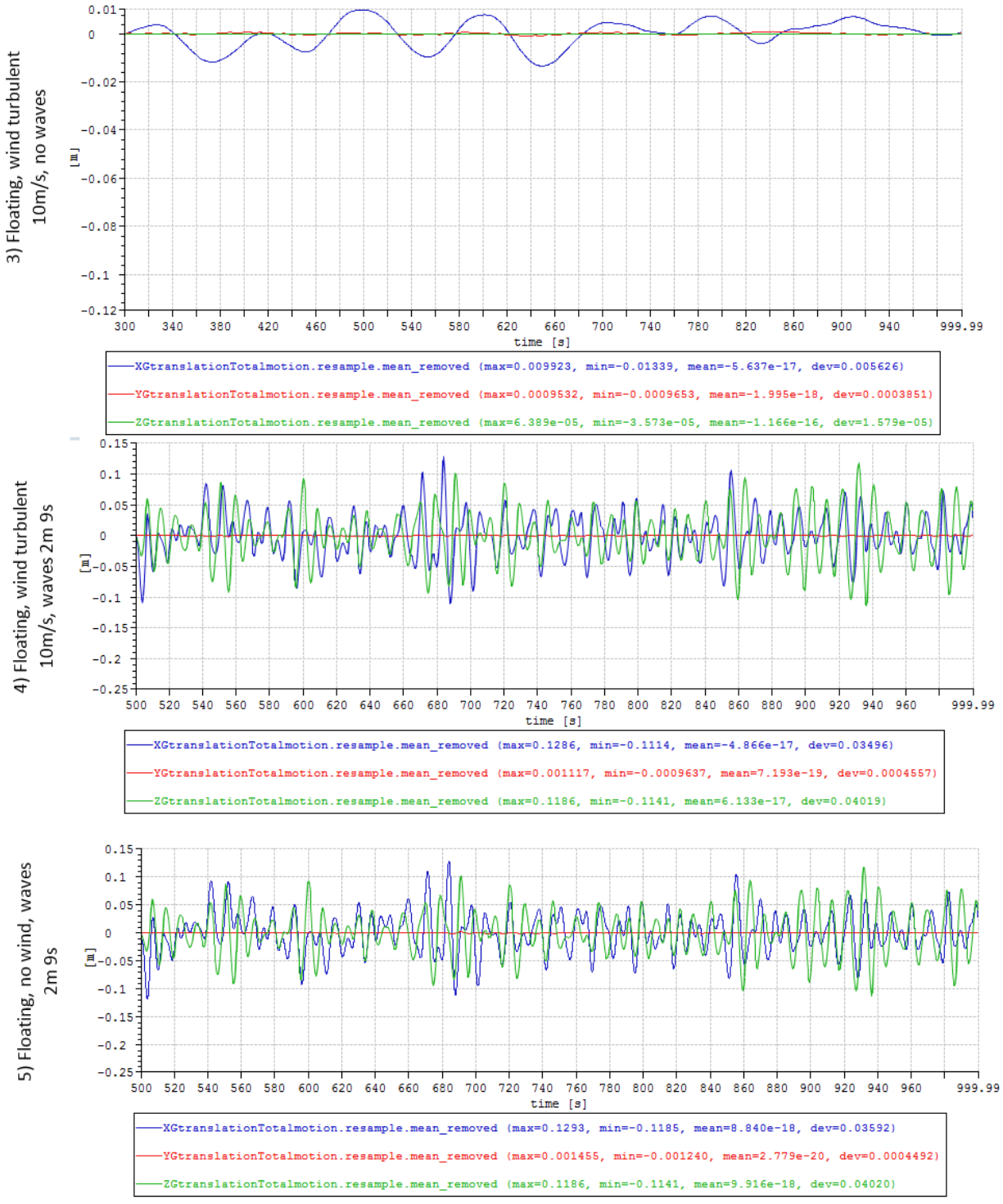

Figure C.6: Translation displacement of the vessel at vessel center for tests 3 to 5. X-component in blue, Y-component in red, Z-component in green

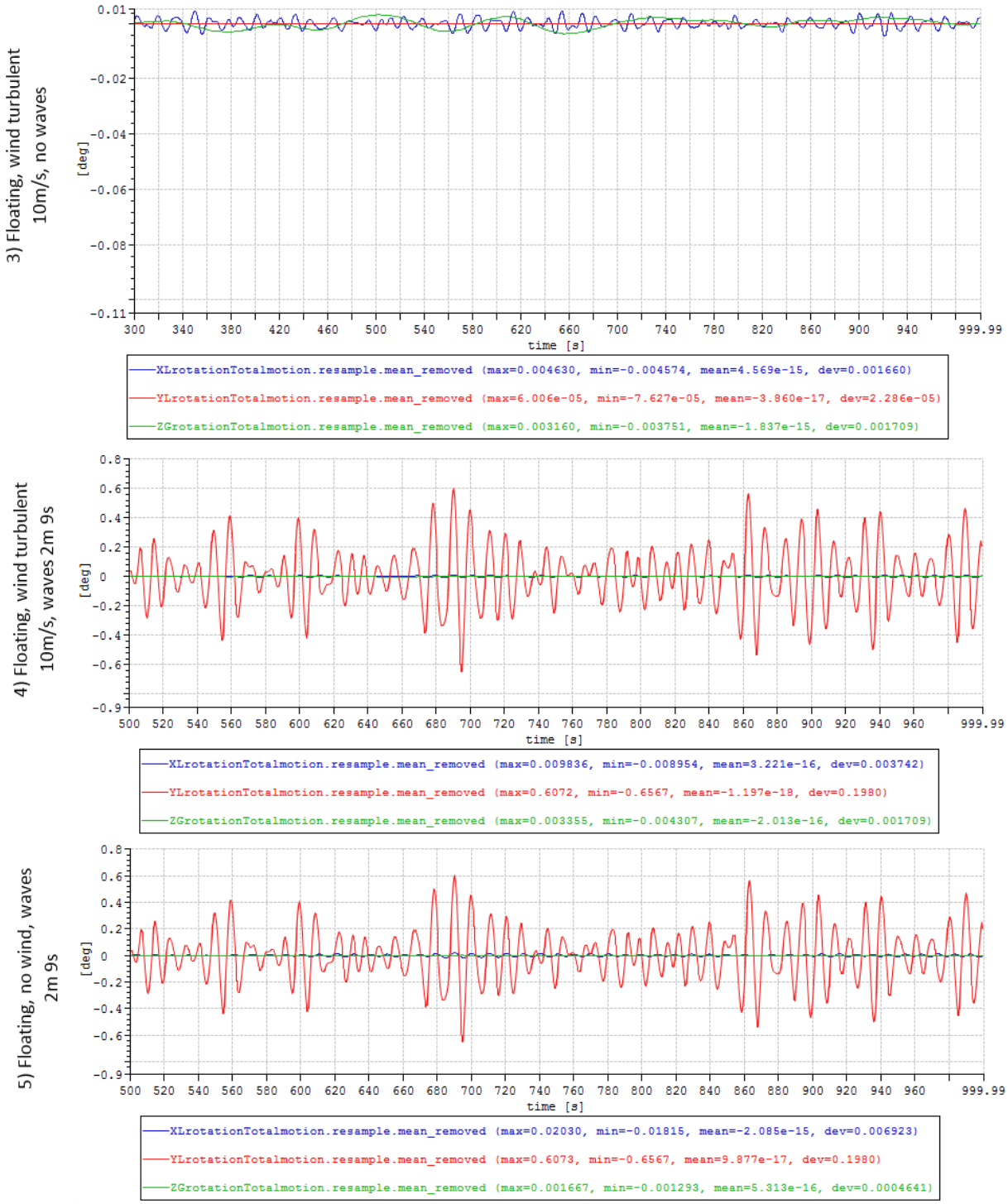

Figure C.7: Rotational displacement of the vessel for tests 3 to 5. X-component in blue, Y-component in red, Z-component in green

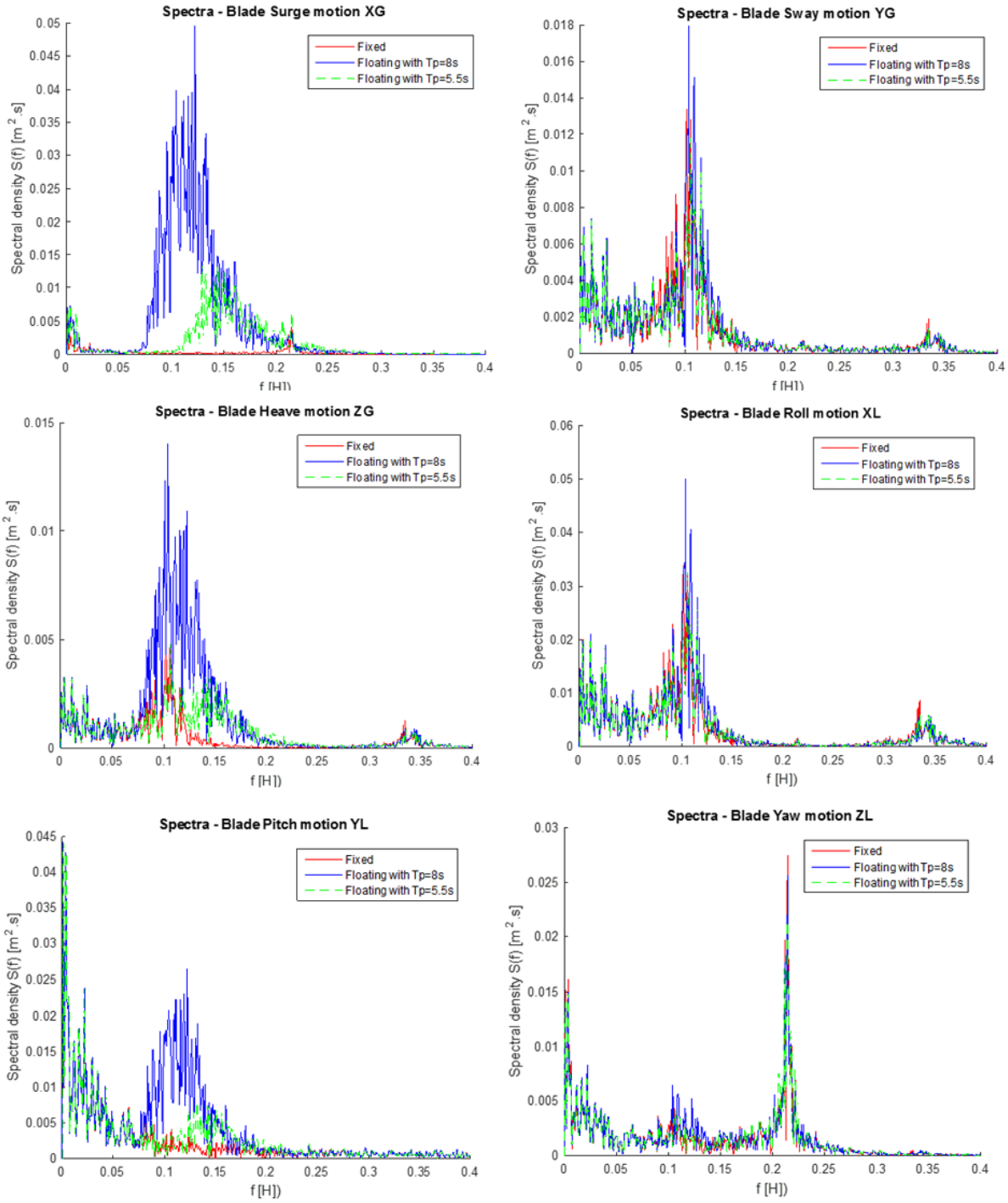

Figure C.8: Spectra for Blade CoG motions

Bibliography

Acero, W. G., Li, L., Gao, Z., and Moan, T. (2016). Methodology for assessment of the operational limits and operability of marine operations. *Ocean Engineering*.

Ahn, D., chul Shin, S., young Kim, S., Kharoufi, H., and cheol Kim, H. (2016). Comparative evaluation of different offshore wind turbine installation vessels for korean westesouth wind farm. *ScienceDirect*.

Bak, C., Zahle, F., Bitsche, R., Kim, T., Yde, A., Henriksen, L. C., Natarajan, A., and Hansen, M. H. (2013). Design and performance of a 10 mw wind turbine. Technical report, J. Wind Energy.

Cheng, Z., Madsen, H., Gao, Z., and Moan, T. (2016). Aerodynamic modeling of floating vertical axis wind turbines using the actuator cylinder flow method. *Energy Procedia*.

De Groot, K. (2015). A novel method for installing offshore wind turbine blades with a floating vessel. Master's thesis, TU Delft.

EWEA (2013). Deep water -the next step for offshore wind energy. Technical report, European Wind Energy Association.

EWEA (2016). The european offshore wind industry - key trends and statistics 2015. Technical report, European Wind Energy Association.

Gaunaa, M., Bergami, L., Guntur, S., and Zahle, F. (2014). First-order aerodynamic and aeroelastic behavior of a single-blade installation setup. *Journal of Physics: Conference Series*, (524).

Gawen, P. (2014). Dynamic soil structure of offshore wind turbines and long term performance prediction: Linking scaled model test results to prototype prediction via element tests. *VJ Tech*.

IEC (2005). International standard 61400-1, wind turbines, part 1: Design requirements.

Kuijken, L. (2015). Single blade installation for large wind turbines in extreme wind conditions. Master's thesis, European Wind Energy Master - EWEM.

Madland, S. (2012). Dynamic analysis for the installation of offshore wind turbine foundations. Master's thesis, University of Stavanger.

MARINTEK (2015a). Simo-theory manual.

MARINTEK (2015b). Simo-user manual.

Tveiten, C. K., Albrechtsen, E., Heggset, J., Hofmann, M., Jersin, E., Leira, B., and Norddal, P. K. (2015). Hse challenges related to offshore renewable energy. *SINTEF Technology and Society*.

Uraz, E. (2011). Offshore wind turbine transportation and installation analyses- planning optimal marine operations for offshore wind projects. Master's thesis, Gotland University.

Zhao, Y., Cheng, Z., Sandvik, P. C., Gao, Z., and Moan, T. (2017). An integrated dynamic analysis method for simulating installation of a single blade for offshore wind turbines. *Centre for Autonomous Marine Operations and Systems AMOS*.